A Universal Theory of Spin Squeezing

Maxwell Block,[1,*] Bingtian Ye,[1,*] Brenden Roberts,[1] Sabrina Chern,[1] Weijie Wu,[2] Zilin Wang,[2] Lode Pollet,[3,4] Emily J. Davis,[2] Bertrand I. Halperin,[1] and Norman Y. Yao[1,2]

[1]*Department of Physics, Harvard University, Cambridge, MA 02139, USA*
[2]*Department of Physics, University of California, Berkeley, CA 94720, USA*
[3]*Arnold Sommerfeld Center for Theoretical Physics, University of Munich, Theresienstr. 37, 80333 München, Germany*
[4]*Munich Center for Quantum Science and Technology (MCQST), Schellingstr. 4, 80799 München, Germany*

We provide extensive numerical and analytic evidence for the following conjecture: Any Hamiltonian exhibiting finite temperature, easy-plane ferromagnetism (XY order) can be used to generate scalable spin squeezing, and thus to perform quantum-enhanced sensing. Our conjecture is guided by a deep connection between the quantum Fisher information of pure states and the spontaneous breaking of a continuous symmetry. We demonstrate that spin-squeezing exhibits a phase diagram with a sharp transition between scalable squeezing and non-squeezing. This transition coincides with the equilibrium phase boundary for XY order at a finite temperature. In the scalable squeezing phase, we predict a sensitivity scaling as $N^{-\frac{7}{10}}$, between the standard quantum limit, $N^{-\frac{1}{2}}$, and that achieved in all-to-all coupled easy-plane spin models, $N^{-\frac{5}{6}}$. Our results provide fundamental insight into the landscape of Hamiltonians that can be used to generate metrologically useful quantum states.

Quantum enhanced metrology makes use of many-body entangled states to perform measurements with greater precision than would be possible using only classically correlated particles [1–5]. Identifying states suitable for quantum metrology is a delicate challenge: nearly all states in Hilbert space are highly entangled, but almost none of them exhibit the structured entanglement required for enhanced sensing. Indeed, only a handful of metrologically useful quantum states are typically discussed, e.g. GHZ states [6–10], Dicke states [11–15], and squeezed states [16–21]. Identifying universal principles for adding to this list remains an important challenge, especially in the context of efficiently preparing metrologically useful states from un-entangled product states.

One such principle, which is particularly powerful, stems from the observation that the quantum Fisher information (QFI) for pure states is fundamentally connected to spontaneous symmetry breaking. On the one hand, the QFI characterizes the maximum sensitivity of a given quantum state, $|\psi\rangle$, to a specific perturbation, $\hat{\mathcal{O}} = \sum_i \hat{\mathcal{O}}_i$ and simply reduces to the variance of $\hat{\mathcal{O}}$ [22]. On the other hand, spontaneous symmetry breaking, with order parameter $\hat{\mathcal{O}}$, corresponds to the existence of long-range connected correlations and thus a variance which scales quadratically in system size. This latter fact immediately implies that any pure quantum state exhibiting long-range order can be utilized to perform Heisenberg-limited sensing [23]. Combining these considerations with the eigenstate thermalization hypothesis—which asserts that generic quantum dynamics cause few-body observables to reach thermal equilibrium [24–26]—suggests a broad and simple guiding principle for preparing metrologically useful states from product states: Identify a Hamiltonian, H, exhibiting finite temperature order. Then, find an unentangled state $|\psi_0\rangle$ whose effective temperature is below T_c and time evolve.

The efficiency of this strategy depends crucially on the nature of the symmetry being broken. For discrete symmetries, it takes an exponentially long time (in system size) to develop a large QFI (see Methods). For continuous symmetries however, a large QFI can develop significantly faster (i.e. in polynomial time) [27, 28]. To this end, we apply the above principle to the case of $U(1)$ symmetry breaking and provide extensive numerical and analytic evidence for the following remarkable conjecture: Finite-temperature easy-plane ferromagnetism (i.e. XY magnets) enables the preparation of states with large QFI, specifically in the form of scalable spin squeezing.

Our main results are threefold. First, we establish a phase diagram for spin squeezing (Fig. 1), with a sharp transition distinguishing scalable squeezing from non-squeezing. Second, we argue that this transition occurs precisely when the effective temperature of the initial state $|\psi_0\rangle$ equals the critical temperature for continuous symmetry breaking (CSB) [29]. Finally, we show that the squeezing manifests a novel scaling with system size—whose origin is extremely subtle—that leads to a phase sensitivity $\sim N^{-\frac{7}{10}}$, between the standard quantum limit ($\sim N^{-\frac{1}{2}}$) and the Heisenberg limit ($\sim N^{-1}$). Intriguingly, for parametrically long time-scales in the inverse temperature of the initial state, we observe a sensitivity scaling as $\sim N^{-\frac{5}{6}}$, matching that achieved in all-to-all coupled easy-plane spin models, i.e., so-called one-axis twisting (OAT) models [16]. Our results are based on the assumption that after a short initial period of time, the long-wavelength, low-frequency properties of the system can be described by hydrodynamic equations involving the conserved z-component of the spin-density and the orientation of the magnetization in the x-y plane. While the form of these hydrodynamical equations is fixed, their parameters depend on the microscopic Hamiltonian; to this end, we utilize a variety of approximate numerical methods to investigate both the squeezing dynamics as well as the equilibrium phase diagram of a broad class of easy-plane spin models.

Connecting squeezing to XY magnetism.—To investigate our conjecture, let us consider the paradigmatic family of $U(1)$-symmetric spin Hamiltonians: the long-range $S = 1/2$

* These authors contributed equally to this work.

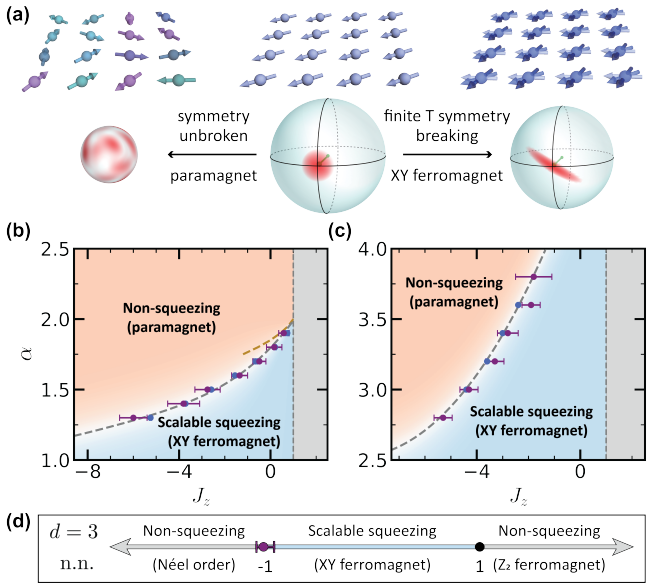

FIG. 1. (a) Schematic depicting the connection between spin squeezing and XY ferromagnetic order. The central panel shows an initial product state polarized in the equatorial plane, with its quantum projection noise (i.e. Wigner quasiprobability distribution) indicated in red. When the effective temperature of the initial state is below the critical temperature for $U(1)$ symmetry breaking (right panel), the system equilibrates to an XY ferromagnet and exhibits scalable squeezing. When the initial state is above the critical temperature, the system equilibrates to a paramagnet, where the total spin length vanishes, precluding spin squeezing (left panel). (b,c) Phase diagrams for scalable spin squeezing as a function of the XXZ anisotropy, J_z, and the interaction power-law, α, in dimensions $d = 1, 2$. The location of the squeezing phase transition is computed via DTWA (purple markers). In 1D, the location of the XY ordering transition is computed via imaginary time evolution on matrix product states (blue markers, dashed line guide to the eye), while in 2D, the transition is computed via quantum Monte Carlo (blue markers, dashed line guide to the eye). In both cases, the phase boundaries are in close agreement. The gold dashed line in (b) corresponds to the phase boundary computed analytically from spin-wave theory (see Methods). (d) Phase diagram for scalable squeezing as a function J_z for a nearest-neighbor interacting system in dimension $d = 3$. For $|J_z| > 1$, there is Néel or Ising order (rather than CSB), so squeezing does not occur.

XXZ model

$$H_{\rm XXZ} = -\sum_{i<j} \frac{J_\perp(\sigma_i^x\sigma_j^x + \sigma_i^y\sigma_j^y) + J_z\sigma_i^z\sigma_j^z}{r_{ij}^\alpha}, \qquad (1)$$

where $J_\perp/J_z$ characterizes the easy-plane anisotropy and α is the long-range power law. This class of Hamiltonians is the most natural and widely studied generalization of one-axis twisting [30–36] and is also realized in a number of quantum simulation platforms ranging from solid-state spins and optical-lattice Hubbard models to ultracold polar molecules and Rydberg atom arrays [27, 37–42]. While our conjecture applies in all dimensions,we note that in $d = 1, 2$ [Fig. 1(b,c)] finite-temperature continuous symmetry breaking is only possible for sufficiently long-range power laws whereas in $d = 3$ [Fig. 1(d)] it is possible even with nearest-neighbor interaction [43–45]. To establish the connection between squeezing and order we utilize a variety of numerical tools: the discrete truncated Wigner approximation (DTWA) for spin-squeezing dynamics, imaginary time evolution of matrix product states for diagnosing $U(1)$ symmetry breaking order in $d = 1$, and path integral quantum Monte Carlo for diagnosing order in $d = 2, 3$ [46, 47]. In addition, whenever possible, our numerical results are carefully benchmarked with a combination of time-dependent variational Monte Carlo, Krylov subspace methods, and exact diagonalization [48].

Let us begin in $d = 1$ with ferromagnetic XY interactions (hereafter, we set $J_\perp = 1$). For $J_z > 1$, the Hamiltonian lies in the easy-axis regime and can only exhibit discrete (Ising) symmetry breaking; this immediately rules out the possibility of quantum-enhanced sensing at accessible time scales [Fig. 1(b)]. For $J_z < 1$, the system can exhibit continuous symmetry breaking at finite temperatures provided that $\alpha < 2$. Consider the parameter space with weak power laws and strong antiferromagnetic Ising interactions [pink, Fig. 1(b)]. Taking our initial state as the fully polarized coherent spin state in the x direction, $|x\rangle = |\rightarrow\cdots\rightarrow\rangle$, we evolve under $H_{\rm XXZ}$ and measure both the average XY magnetization, $m_{\rm xy} = [\langle X^2 + Y^2\rangle/N^2]^{1/2}$ and the squeezing parameter $\xi^2 \equiv N \min_{\hat{n}\perp\hat{x}} {\rm Var}[\hat{n}\cdot\vec{S}]/\langle X\rangle^2$ (which entails a phase sensitivity of $\Delta\phi = \sqrt{\frac{\xi^2}{N}}$); here, $X = \frac{1}{2}\sum_i \sigma_i^x$ (with Y and Z defined analogously) and $\vec{S} = (X, Y, Z)$. As a function of increasing system size, the magnetization decays to zero, indicating thermalization to a disordered state [Fig. 2(a)]. Meanwhile, the squeezing parameter, which quantifies the enhancement in sensitivity over the initial coherent state, exhibits marginal improvement at short times. However, this improvement *does not* scale with system size and at late times, ξ^2 steadily worsens [Fig. 2(a)].

The dynamics in the opposite parameter space [blue, Fig. 1(b)], with strong power laws and weak antiferromagnetic Ising interactions is markedly distinct. Here, the XY magnetization rapidly equilibrates to a system-size-independent value (i.e. the order parameter), indicating robust continuous symmetry breaking [Fig. 2(b)]. Accompanying the presence of order is the existence of scalable spin squeezing, where the optimal squeezing value improves with system size (i.e. $\xi^2_{\rm opt} \sim N^{-\nu}$ with $\nu > 0$) and occurs at later and later times [Fig. 2(b)]. This is precisely reminiscent of the behavior in the one-axis-twisting model, where $\xi^2_{\rm opt} \sim N^{-\frac{2}{3}}$.

The essence of our conjecture is already captured by the above dichotomy: thermalizing to a disordered state correlates with non-squeezing, while thermalizing to an ordered state correlates with scalable squeezing. But our conjecture is stronger than claiming an association between squeezing and finite-temperature order; rather, we argue that they are two facets of the same phase. To more quantitatively investigate this, for each point in parameter space, $\{\alpha, J_z\}$, we extract the optimal squeezing and the late-time XY magnetization as a function of system size (see Methods for details). Depicted in Figure 2(c), is a cut across parameter space, fixing $\alpha = 1.5$ and varying J_z. For large, negative J_z, the XY magnetization plateau vanishes with increasing system size. As J_z becomes

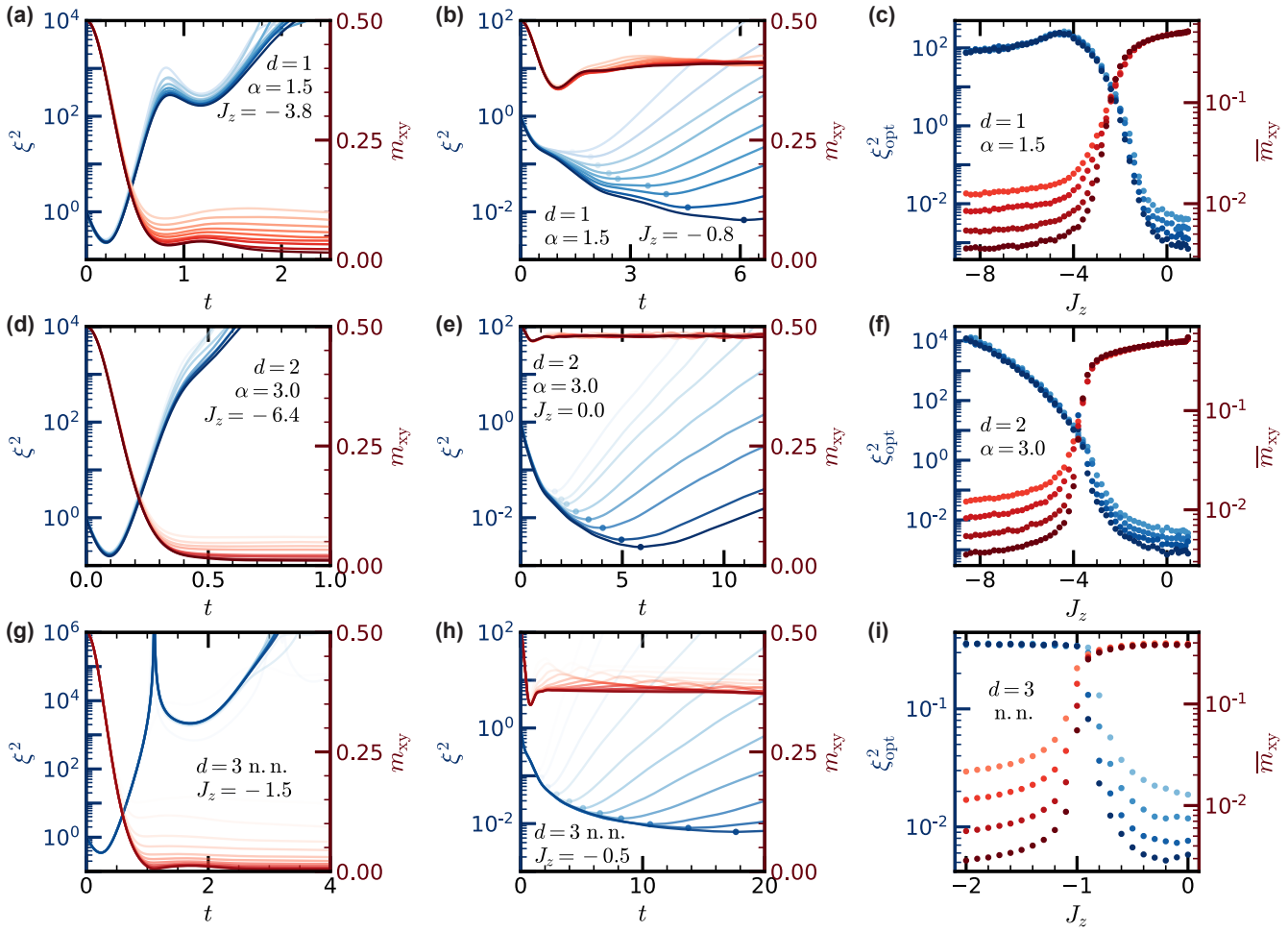

FIG. 2. (a,b) Depicts the dynamics ($d = 1$) of the squeezing parameter ξ^2 (blue) and the XY order, $m_{\rm xy}$ (red), as a function of time, upon quenching from an initial product state polarized in the $\hat{x}$ direction. Opacity increases with system size (from $N = 10^2 - 10^4$). In the paramagnetic phase (a), $m_{\rm xy}$ decays to zero, while the squeezing parameter does not improve with system size. In the ferromagnetic phase (b), $m_{\rm xy}$ plateaus to a finite value, and the squeezing parameter scales with system size. (d,e) and (g,h) Depict the analogous dynamics for $d = 2$ and $d = 3$, with system sizes $N = 10^2 - 10^4$ and $N = 10^2 - 10^5$. (c) Fixing $\alpha = 1.5$ in $d = 1$, the optimal squeezing parameter (blue) and the plateau value of the XY order (red) are shown as a function of J_z. Darker color shades correspond to larger system sizes (with $N = 5 \cdot 10^3 - 5 \cdot 10^4$). In the paramagnetic phase (large J_z magnitude), the XY order decays with increasing system size, while in the ferromagnetic phase the XY order is independent of system size, indicating a phase transition at $J_c \approx -2.4$. The behavior of the optimal squeezing exhibits a separatrix at the same value of J_c, where it transitions from being system-size independent to scaling with N. (f) and (i) Depict analogous J_z-cuts in the phase diagrams for $d = 2$ fixing $\alpha = 3.0$ (with $N = 5 \cdot 10^3 - 5 \cdot 10^4$) and $d = 3$ (with $N = 2 \cdot 10^3 - 10^5$). Calculations were performed using the DTWA approximation.

weaker and enters the ferromagnetic regime, there is a clear separatrix — indicative of a symmetry-breaking phase transition — where the value of the magnetization plateau becomes system-size independent. Remarkably, the scaling behavior of the optimal squeezing is in perfect correspondence with the magnetization. In the region where the magnetization vanishes, the squeezing does not scale. In the opposite regime, the optimal squeezing exhibits its own separatrix and shows a pronounced scaling with system size.

This change in scaling provides a simple method to determine the location of the squeezing transition: for each value of J_z, we fit $\xi^2_{\rm opt} \sim N^{-\nu}$ and associate the critical point, $J_{\rm c}$, with the onset of $\nu \gtrsim 0$ (see Methods for details). Repeating this procedure as a function of α leads to the squeezing phase boundary demarcated by the purple data points in Figure 1(b). Similarly, one can also define a $U(1)$ symmetry-breaking phase boundary, which occurs when the effective temperature of the initial state, $|x\rangle$, crosses the critical temperature for XY order. To identify this phase boundary, we cool an infinite temperature (purified) matrix product state to the energy density of the $|x\rangle$-state using imaginary time evolution under $H_{\rm XXZ}$. A finite-size scaling analysis then yields the XY-ordering phase boundary demarcated by the blue data points in Figure 1(b). That the squeezing and ordering phase boundaries coincide within error bars not only provides evidence for our conjecture but also shows that the DTWA is

remarkably accurate in the region of the transition [49].

A few additional remarks are in order. First, one can analytically estimate the CSB phase boundary within spin-wave theory [dashed gold line, Fig. 1(b)]. A particularly nice feature of this analysis is that it predicts the observed behavior, where J_c approaches the Heisenberg point as $\alpha \to 2$ (beyond which there is no finite temperature order). Second, we demonstrate precisely the same correspondence between squeezing and order in $d = 2$ [Fig. 2(d-f)] and in $d = 3$ [Fig. 2(g-i)] (see Methods). Interestingly, the topology of the squeezing phase diagram in $d = 2$ is slightly distinct — in particular, even as $\alpha \to 4$ (beyond which there is no finite temperature order), J_c does not approach the Heisenberg point, so there remains a finite interval $-1 \lesssim J_z < 1$ where scalable squeezing occurs. Third, in $d = 1, 2$, scalable squeezing disappears as J_z decreases because the temperature of the initial $|x\rangle$-state becomes higher than the critical temperature; however, in $d = 3$, at least for the nearest-neighbor model we consider, the squeezing disappears for $J_z < -1$, because the continuous-symmetry-breaking XY ferromagnet is replaced by discrete-symmetry-breaking Néel order.

Finally, a semiclassical view of the dynamics provides the essential intuition for the connection between squeezing and order. In this framework, the initial state $|x\rangle$ is viewed as a Wigner quasi-probability distribution on the total-spin phase space, represented by a sphere of radius $|S| = N/2$ [middle, Fig. 1(a)]. In the all-to-all coupled case ($\alpha \to 0$), one-axis twisting dynamics yield squeezing by causing slices from this distribution to rotate about the $\hat{z}$-axis with an angular velocity proportional to total $Z = \frac{1}{2}\sum_i \sigma_i^z$. Our key insight is that even in the power-law coupled case with $\alpha > d$, or the short-ranged case with $d \geq 3$, a similar picture should hold as long as the state remains ordered. Specifically, if the effective temperature of $|x\rangle$ is below the equilibrium CSB critical temperature, then $m_{\text{xy}}^2 > 0$ [Fig 2(b,e,h)] and the initial Wigner distribution will simply relax, on a microscopic timescale independent of N, to a slightly distorted distribution on a smaller phase space of radius $m_{\text{xy}}N$ [Fig 1(a), right]. This "dressed" distribution will then evolve qualitatively similarly to the all-to-all coupled case.

Scalable squeezing in the XY magnet.—Based upon the semi-classical intuition from above, one might naively expect that squeezing in the finite-temperature XY magnet should exhibit the same scaling as in one-axis twisting. However, this is oversimplified. Perhaps the easiest way to see this is to consider the conditional variance of Y given Z, denoted as $\text{Var}[Y|Z]$, within the semi-classical approximation. As illustrated in Fig. 3(a), for one-axis twisting, $\text{Var}[Y|Z]$ is a constant of motion: each Z-slice of the probability distribution rotates rigidly about the sphere. But in a system that does not conserve total spin, e.g. H_{XXZ}, the conditional variance will increase as a function of time [Fig. 3(a)]; indeed, a simple hydrodynamic model suggests that $Y|Z$ evolves diffusively, so $\text{Var}[Y|Z]$ grows linearly in time with a slope that depends strongly on temperature (see Methods). To understand the impact of this variance growth, we note that (within a semi-classical picture) :

$$\xi^2(t) \approx \frac{\text{Var}[Y|Z]/N}{4m_{\text{xy}}^4(\chi t)^2} + \frac{(\chi t)^4}{24 m_{\text{xy}}^2 N^2}, \tag{2}$$

where χ is the effective one-axis twisting strength, related to the z-axis spin susceptibility (see Methods and [16, 28]). When the conditional variance remains constant (i.e. one-axis twisting), optimizing over t yields $\xi^2 \sim N^{-\frac{2}{3}}$ (leading to a phase sensitivity $\sim N^{-\frac{5}{6}}$). However, linear growth of the conditional variance predicts instead that $\xi^2 \sim N^{-\frac{2}{5}}$ (leading to a phase sensitivity $\sim N^{-\frac{7}{10}}$).

At low temperatures, the slope of the variance growth is small, suggesting that the asymptotic scaling behavior will only be observed at extremely large system sizes. To control the temperature, we introduce an additional tuning parameter (which is particularly relevant to experiments [27]): the polarization of the initial state. For polarization p, we initialize a product state, where each spin points along $+x$ with probability $(1 + p)/2$ and along $-x$ with probability $(1 - p)/2$. This polarization tunes the effective temperature of the initial state. At low temperatures ($p \approx 1$), the squeezing appears to scale as $\sim N^{-\frac{2}{3}}$ [Fig. 3(b,c)]. At intermediate temperatures near the transition, the squeezing scales as $\sim N^{-\frac{2}{5}}$ over multiple decades in system size [Fig. 3(b,c)]. As soon as the polarization tunes the temperature above T_c, a "gap" emerges in the scaling behavior and ξ^2 becomes independent of system size [Fig. 3(b,c)]. We note that the low-temperature scaling of $N^{-\frac{2}{3}}$ is not expected to hold as $N \to \infty$; rather, as shown in Fig. 3(d), the scaling will eventually cross over to the asymptotic behavior of $N^{-\frac{2}{5}}$.

Although our semi-classical analysis provides a coarse-grained explanation for the difference between the scaling of the squeezing in all-to-all versus finite-range interacting systems, the microscopic dynamics are fundamentally quantum mechanical. This raises the question: is the asymptotic squeezing scaling also modified in the true quantum dynamics?

To answer this, we begin by developing a quantum interpretation of $\text{Var}[Y|Z]$. Intuitively, $\text{Var}[Y|Z]$ can also be computed as the remaining variance of Y *after* one has counter-rotated each Z-slice of the probability distribution back to its original mean. Crucially, both semi-classically and quantum mechanically, this counter-rotation can be realized by evolving the system under one-axis twisting. From this perspective, the quantum analog of $\text{Var}[Y|Z]$ is closely connected to a Loschmidt echo of the form:

$$\text{Var}_{\text{q}}[Y|Z] = \langle x|\, e^{it[H_{\text{XXZ}} - \chi \frac{\hat{Z}^2}{N}]}\, \hat{Y}^2\, e^{-it[H_{\text{XXZ}} - \chi \frac{\hat{Z}^2}{N}]}\, |x\rangle\,. \tag{3}$$

Since the thermalization induced by the XXZ-dynamics cannot be perfectly undone by one-axis twisting, $\text{Var}_{\text{q}}[Y|Z]$ will grow in time until saturating at its equilibrium value of $m_{\text{xy}}^2 N^2/2$. In Fig. 3(e), we illustrate the variance growth for a 1D system at $\alpha = 1.5, J_z = 0$ and find that (at least in this parameter regime), $\text{Var}_{\text{q}}[Y|Z]$ for $N = 18$ indeed agrees

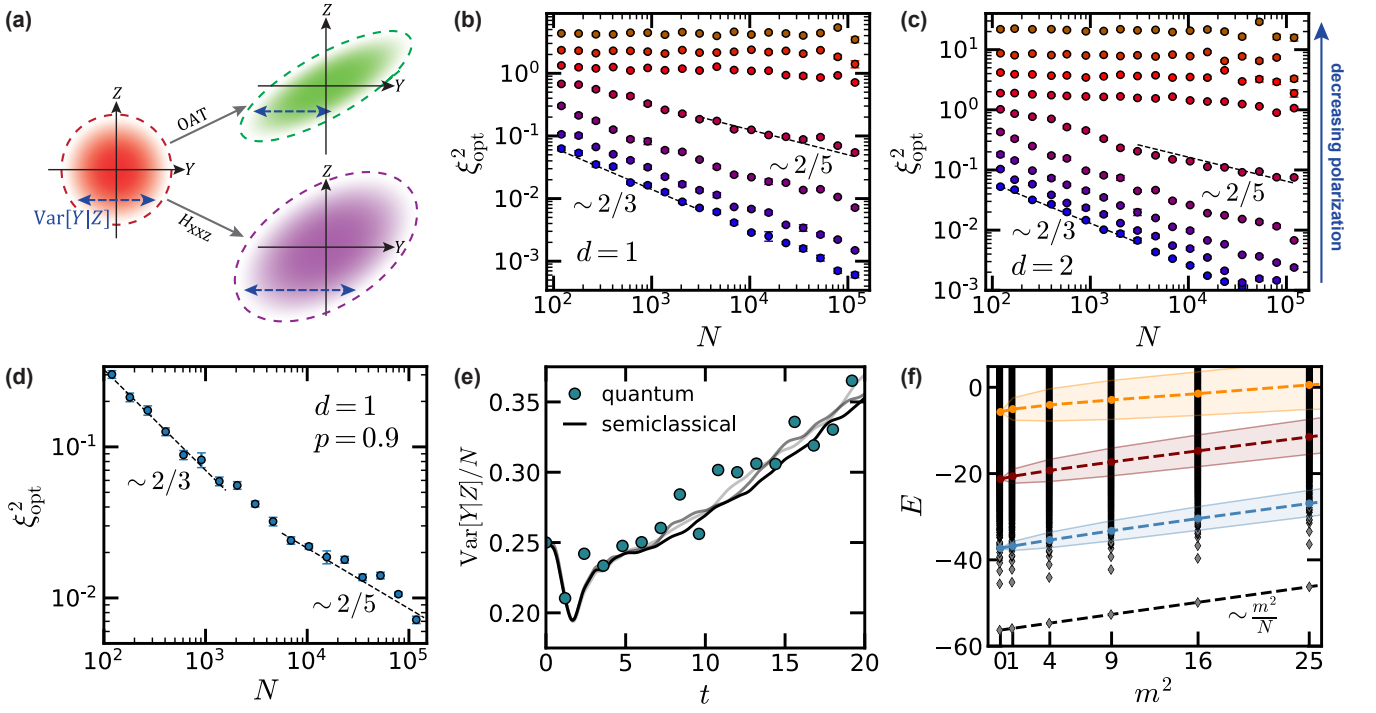

FIG. 3. (a) Schematic illustrating the dynamics of the conditional variance in the OAT model (green) and the XXZ model (purple) at finite temperature. In the OAT model, $\mathrm{Var}[Y|Z]$ remains constant, while in the XXZ model, the conditional variance exhibits an additional linear growth in time. (b) DTWA simulations depicting the optimal squeezing as a function of system size. The polarization of the initial state decreases from $p = 1.0$ (blue) to $p = 0.7$ (red); this tunes the effective temperature of the initial state across the critical temperature for XY order. As the polarization decreases, the scaling changes sharply from $N^{-2/5}$ to N^0. At lower effective temperatures ($p \approx 1$), the asymptotic $N^{-2/5}$ scaling emerges only for larger system sizes. (c) Depicts the analogous results for $d = 2$ where the polarization ranges from $p = 1.0$ (blue) to $p = 0.6$ (red). (d) Shows a crossover in the scaling behavior for $d = 1$ with polarization $p = 0.9$. At small system sizes, the squeezing scales as $N^{-2/3}$ consistent with OAT. However, at larger system sizes, the scaling crosses over to the asymptotic prediction of $N^{-2/5}$. (e) In the squeezing phase ($\alpha = 1.5, J_z = 0$), both semi-classical DTWA simulations (for $N = 1000, 2000, 4000$ with $Z = 0$) and exact quantum dynamics ($N = 18$) show the conditional variance growing linearly in time. Their quantitative agreement lends support to the quantum-mechanical origin of the variance growth. (f) Diamonds depict the spectrum of $H_{\rm XXZ}$ at $\alpha = 1.5, J_z = 0$ for $N = 24$. The eigenstates in different m-sectors are connected by total-spin raising and lowering operators. The ground state manifold exhibits a so-called "Anderson tower" structure where the energies scale as $E \sim m^2/N$ [50]. At finite temperatures, this manifold becomes a distribution with an approximate "Anderson tower" structure: The set of states that are connected to a given initial finite-energy state upon successive applications of the total-spin raising or lowering operator will have a distribution of energies, which is illustrated here for three initial states with $m = 0$ but differing energies E_0. The dashed lines, which indicate the mean values of the distributions, exhibit the same scaling, $E - E_0 \sim m^2/N$, but the variance (shaded region) increases with E_0 .

extremely well with the semi-classical conditional variance in the thermodynamic limit [Fig. 3(e)].

Interestingly, a complementary picture for the behavior of $\mathrm{Var_q}[Y|Z]$ emerges from the spectral structure of $H_{\rm XXZ}$. The ground states of adjacent magnetization sectors of $H_{\rm XXZ}$ are connected by the total spin raising and lower operator. Taken together, they form a so-called "Anderson tower" with energies scaling as $E \sim m^2/N$ [Fig. 3(f)]. In the one-axis-twisting model, squeezing arises from the fact that the *entire* spectrum exhibits this "Anderson tower" structure. By contrast, at finite energy densities, the spectrum of $H_{\rm XXZ}$ features only approximate "Anderson towers": the raising and lowering operator connect a given eigenstate in an m-sector to several others in adjacent sectors, leading to a distribution of energies [Fig. 3(f)]. It is precisely the variance of this distribution which drives thermalization in the XXZ model, and thus the growth of $\mathrm{Var_q}[Y|Z]$.

Outlook.—Our work opens the door to a number of intriguing directions. First, while we have established the presence of a phase transition between scalable squeezing and non-squeezing, the nature of this transition remains an open question. In particular, whether the transition can be analyzed within the same equilibrium paradigm as the CSB transition, or whether it should be described as a non-equilibrium transition associated with the dynamics is unclear. Second, our framework connecting the quantum Fisher information of pure states to spontaneous symmetry breaking suggests a new strategy for finding (and preparing) metrologically useful states. However, the ability to prepare a state with large QFI does not immediately imply that one can straightforwardly utilize it for sensing; indeed, in the most general case, it is necessary to time-reverse the dynamics, in order to extract the metrological signal [51–53]. In the case of $U(1)$ symmetry breaking, the emergence of squeezing *does* guarantee a sim-

ple way to harness the metrological gain [17]. It is intriguing to ask whether this fortuitous circumstance holds in general. Relatedly, it would be interesting to explore the breaking of non-Abelian continuous symmetries, where one might naturally be sensitive to perturbations beyond scalar fields. Finally, our work implies that scalable squeezing can be realized in a variety of quantum simulation platforms with dipolar interactions [27, 37, 40, 41, 54, 55]. For example, ultracold polar molecules in an optical lattice as well as Rydberg atoms in a tweezer array can both implement the two-dimensional dipolar XY model, which is deep in the scalable squeezing phase. The discovery of optically-active spin defects in 2D quantum materials [42, 56, 57] as well as advances in delta-doped crystal growth [58, 59] also suggest a route toward spin squeezing in the solid state; in this setting, the robustness of easy-plane ferromagnetism to the positional disorder of the underlying spin defects is crucial.

Acknowledgements–We gratefully acknowledge the insights of Ehud Altman, Joel Moore, Mike Zaletel, Chris Laumann and Francisco Machado. This work was support by the Army Research Office via grant number W911NF-21-1-0262 and through the MURI program (grant number W911NF-20-1-0136), by the U.S. Department of Energy, Office of Science, National Quantum Information Science Research Centers, Quantum Systems Accelerator (QSA), by the David and Lucile Packard foundation, and by the A. P. Sloan foundation. E.J.D. acknowledges support from the Miller Institute for Basic Research in Science. M.B. acknowledges support through the Department of Defense (DoD) through the National Defense Science and Engineering Graduate (NDSEG) Fellowship Program. L.P. acknowledges support from FP7/ERC Consolidator Grant QSIMCORR, No. 771891, and the Deutsche Forschungsgemeinschaft (DFG, German Research Foundation) under Germany's Excellence Strategy – EXC-2111 – 390814868, as well as the Munich Quantum Valley, which is supported by the Bavarian state government with funds from the Hightech Agenda Bayern Plus. MPS simulations make use of the TenPy and ITensor libraries [47, 60] and QMC simulations make use of the ALPSCore libraries [61, 62].

[1] Giovannetti, V., Lloyd, S. & Maccone, L. Advances in quantum metrology. *Nature Photonics* **5**, 222–229 (2011). URL https://www.nature.com/articles/nphoton.2011.35.

[2] Degen, C., Reinhard, F. & Cappellaro, P. Quantum sensing. *Reviews of Modern Physics* **89**, 035002 (2017). URL http://link.aps.org/doi/10.1103/RevModPhys.89.035002.

[3] Schnabel, R., Mavalvala, N., McClelland, D. E. & Lam, P. K. Quantum metrology for gravitational wave astronomy. *Nature Communications* **1**, 121 (2010). URL https://www.nature.com/articles/ncomms1122.

[4] Wasilewski, W. *et al.* Quantum Noise Limited and Entanglement-Assisted Magnetometry. *Physical Review Letters* **104**, 133601 (2010). URL https://link.aps.org/doi/10.1103/PhysRevLett.104.133601.

[5] Leibfried, D. *et al.* Toward Heisenberg-Limited Spectroscopy with Multiparticle Entangled States. *Science* **304**, 1476–1478 (2004). URL https://www.science.org/doi/10.1126/science.1097576.

[6] Bouwmeester, D., Pan, J.-W., Daniell, M., Weinfurter, H. & Zeilinger, A. Observation of Three-Photon Greenberger-Horne-Zeilinger Entanglement. *Physical Review Letters* **82**, 1345–1349 (1999). URL https://link.aps.org/doi/10.1103/PhysRevLett.82.1345.

[7] Pan, J.-W., Bouwmeester, D., Daniell, M., Weinfurter, H. & Zeilinger, A. Experimental test of quantum nonlocality in three-photon Greenberger–Horne–Zeilinger entanglement. *Nature* **403**, 515–519 (2000). URL https://www.nature.com/articles/35000514.

[8] Omran, A. *et al.* Generation and manipulation of Schrödinger cat states in Rydberg atom arrays. *Science* **365**, 570–574 (2019). URL https://www.science.org/doi/10.1126/science.aax9743.

[9] Pogorelov, I. *et al.* Compact Ion-Trap Quantum Computing Demonstrator. *PRX Quantum* **2**, 020343 (2021). URL https://link.aps.org/doi/10.1103/PRXQuantum.2.020343.

[10] Jones, J. A. *et al.* Magnetic Field Sensing Beyond the Standard Quantum Limit Using 10-Spin NOON States. *Science* **324**, 1166–1168 (2009). URL https://www.science.org/doi/10.1126/science.1170730.

[11] Dicke, R. H. Coherence in Spontaneous Radiation Processes. *Physical Review* **93**, 99–110 (1954). URL https://link.aps.org/doi/10.1103/PhysRev.93.99.

[12] Pezzè, L., Smerzi, A., Oberthaler, M. K., Schmied, R. & Treutlein, P. Quantum metrology with nonclassical states of atomic ensembles. *Reviews of Modern Physics* **90**, 035005 (2018). URL https://link.aps.org/doi/10.1103/RevModPhys.90.035005.

[13] Wieczorek, W. *et al.* Experimental Entanglement of a Six-Photon Symmetric Dicke State. *Physical Review Letters* **103**, 020504 (2009). URL https://link.aps.org/doi/10.1103/PhysRevLett.103.020504.

[14] Lücke, B. *et al.* Detecting Multiparticle Entanglement of Dicke States. *Physical Review Letters* **112**, 155304 (2014). URL https://link.aps.org/doi/10.1103/PhysRevLett.112.155304.

[15] Zou, Y.-Q. *et al.* Beating the classical precision limit with spin-1 Dicke states of more than 10,000 atoms. *Proceedings of the National Academy of Sciences* **115**, 6381–6385 (2018). URL https://pnas.org/doi/full/10.1073/pnas.1715105115.

[16] Kitagawa, M. & Ueda, M. Squeezed spin states. *Phys. Rev. A* **47**, 5138–5143 (1993). URL https://link.aps.org/doi/10.1103/PhysRevA.47.5138.

[17] Wineland, D. J., Bollinger, J. J., Itano, W. M. & Heinzen, D. J. Squeezed atomic states and projection noise in spectroscopy. *Physical Review A* **50**, 67–88 (1994). URL https://link.aps.org/doi/10.1103/PhysRevA.50.67.

[18] Hosten, O., Engelsen, N. J., Krishnakumar, R. & Kasevich, M. A. Measurement noise 100 times lower than the quantum-projection limit using entangled atoms. *Nature* **529**, 505–508 (2016). URL https://www.nature.com/articles/nature16176. Number: 7587 Publisher: Nature Publishing Group.

[19] Estève, J., Gross, C., Weller, A., Giovanazzi, S. & Oberthaler, M. K. Squeezing and entanglement in a Bose–Einstein condensate. *Nature* **455**, 1216–1219 (2008). URL https://www.nature.com/articles/nature07332.

[20] Appel, J. *et al.* Mesoscopic atomic entanglement for precision measurements beyond the standard quantum limit. *Proceedings of the National Academy of Sciences* **106**, 10960–10965 (2009). URL https://pnas.org/doi/full/10.1073/pnas.0901550106.

[21] Muessel, W., Strobel, H., Linnemann, D., Hume, D. & Oberthaler, M. Scalable Spin Squeezing for Quantum-Enhanced Magnetometry with Bose-Einstein Condensates. *Physical Review Letters* **113**, 103004 (2014). URL https://link.aps.org/doi/10.1103/PhysRevLett.113.103004.

[22] Braunstein, S. L. & Caves, C. M. Statistical distance and the geometry of quantum states. *Physical Review Letters* **72**, 3439–3443 (1994). URL https://link.aps.org/doi/10.1103/PhysRevLett.72.3439.

[23] We note that for mixed states the QFI is not simply given by the variance of the operator.

[24] Deutsch, J. M. Quantum statistical mechanics in a closed system. *Physical Review A* **43**, 2046–2049 (1991). URL https://link.aps.org/doi/10.1103/PhysRevA.43.2046.

[25] Srednicki, M. Chaos and quantum thermalization. *Physical Review E* **50**, 888–901 (1994). URL https://link.aps.org/doi/10.1103/PhysRevE.50.888.

[26] Rigol, M., Dunjko, V. & Olshanii, M. Thermalization and its mechanism for generic isolated quantum systems. *Nature* **452**, 854–858 (2008). URL https://www.nature.com/articles/nature06838.

[27] Chen, C. *et al.* Continuous Symmetry Breaking in a Two-dimensional Rydberg Array (2022). URL https://arxiv.org/abs/2207.12930.

[28] Comparin, T., Mezzacapo, F. & Roscilde, T. Multipartite entangled states in dipolar quantum simulators. *Phys. Rev. Lett.* **129**, 150503 (2022). URL https://link.aps.org/doi/10.1103/PhysRevLett.129.150503.

[29] Note that the effective temperature of the initial state $|\psi\rangle$, is defined as T such that $\mathrm{Tr}[\exp(-H/T)\ H]/Z = \langle\psi|\, H\, |\psi\rangle$.

[30] Perlin, M. A., Qu, C. & Rey, A. M. Spin squeezing with short-range spin-exchange interactions. *Phys. Rev. Lett.* **125**, 223401 (2020). URL https://link.aps.org/doi/10.1103/PhysRevLett.125.223401.

[31] Comparin, T., Mezzacapo, F. & Roscilde, T. Robust spin squeezing from the tower of states of u(1)-symmetric spin hamiltonians. *Phys. Rev. A* **105**, 022625 (2022). URL https://link.aps.org/doi/10.1103/PhysRevA.105.022625.

[32] Cappellaro, P. & Lukin, M. D. Quantum correlation in disordered spin systems: Applications to magnetic sensing. *Physical Review A* **80**, 032311 (2009). URL https://link.aps.org/doi/10.1103/PhysRevA.80.032311.

[33] Davis, E. J. *et al.* Protecting Spin Coherence in a Tunable Heisenberg Model. *Physical Review Letters* **125**, 060402 (2020). URL https://link.aps.org/doi/10.1103/PhysRevLett.125.060402.

[34] Kwasigroch, M. P. & Cooper, N. R. Bose-Einstein condensation and many-body localization of rotational excitations of polar molecules following a microwave pulse. *Physical Review A* **90**, 021605 (2014). URL https://link.aps.org/doi/10.1103/PhysRevA.90.021605.

[35] Kwasigroch, M. P. & Cooper, N. R. Synchronization transition in dipole-coupled two-level systems with positional disorder. *Physical Review A* **96**, 053610 (2017). URL https://link.aps.org/doi/10.1103/PhysRevA.96.053610.

[36] Rey, A. M., Jiang, L., Fleischhauer, M., Demler, E. & Lukin, M. D. Many-body protected entanglement generation in interacting spin systems. *Physical Review A* **77**, 052305 (2008). URL https://link.aps.org/doi/10.1103/PhysRevA.77.052305.

[37] Davis, E. J. *et al.* Probing many-body noise in a strongly interacting two-dimensional dipolar spin system (2021). URL https://arxiv.org/abs/2103.12742.

[38] Greiner, M., Mandel, O., Esslinger, T., Hänsch, T. W. & Bloch, I. Quantum phase transition from a superfluid to a Mott insulator in a gas of ultracold atoms. *Nature* **415**, 39–44 (2002). URL https://www.nature.com/articles/415039a.

[39] Gross, C. & Bloch, I. Quantum simulations with ultracold atoms in optical lattices. *Science* **357**, 995–1001 (2017). URL https://science.sciencemag.org/content/357/6355/995. Publisher: American Association for the Advancement of Science Section: Review.

[40] Ni, K.-K. *et al.* A high phase-space-density gas of polar molecules. *Science* **322**, 231–235 (2008). URL https://www.science.org/doi/abs/10.1126/science.1163861. https://www.science.org/doi/pdf/10.1126/science.1163861.

[41] Chomaz, L. *et al.* Long-Lived and Transient Supersolid Behaviors in Dipolar Quantum Gases. *Physical Review X* **9**, 021012 (2019). URL https://link.aps.org/doi/10.1103/PhysRevX.9.021012.

[42] Tran, T. T., Bray, K., Ford, M. J., Toth, M. & Aharonovich, I. Quantum emission from hexagonal boron nitride monolayers. *Nature Nanotechnology* **11**, 37–41 (2016). URL http://www.nature.com/articles/nnano.2015.242.

[43] For $\alpha > d$, we can choose $J_\perp = 1$ and let the N go to infinity and maintain finite energy density. For $\alpha < d$, to have a finite energy density we need to let $J_\perp$ go to 0 as N goes to infinity. The all-to-all model is realized when we take $\alpha \to 0$ and $J_\perp = 1/N$. Our analysis is restricted to $\alpha > d$.

[44] Bruno, P. Absence of spontaneous magnetic order at nonzero temperature in one- and two-dimensional heisenberg and XY systems with long-range interactions. *Phys. Rev. Lett.* **87**, 137203 (2001). URL https://link.aps.org/doi/10.1103/PhysRevLett.87.137203.

[45] Maghrebi, M. F., Gong, Z.-X. & Gorshkov, A. V. Continuous Symmetry Breaking in 1D Long-Range Interacting Quantum Systems. *Physical Review Letters* **119**, 023001 (2017). URL https://link.aps.org/doi/10.1103/PhysRevLett.119.023001. Publisher: American Physical Society.

[46] Schachenmayer, J., Pikovski, A. & Rey, A. M. Many-body quantum spin dynamics with monte carlo trajectories on a discrete phase space. *Phys. Rev. X* **5**, 011022 (2015). URL https://link.aps.org/doi/10.1103/PhysRevX.5.011022.

[47] Hauschild, J. & Pollmann, F. Efficient numerical simulations with Tensor Networks: Tensor Network Python (TeNPy). *SciPost Physics Lecture Notes* 005 (2018). URL https://scipost.org/10.21468/SciPostPhysLectNotes.5.

[48] See Supplemental Material at [URL will be inserted by publisher].

[49] We note that DTWA dynamics cannot accurately capture the short-range spin fluctuations (after local equilibration) deep in

the quantum regime, i.e. where the effective temperature of the initial state $T \ll J_\perp$. However, this is of little consequence: for $T \ll J_\perp$, finite temperature effects are important only for very long time-scales at systems sizes beyond our power to investigate. Close to the phase transition, where T is of order $J_\perp$, our results suggest that the semiclassical description is more accurate.

[50] Tasaki, H. Long-Range Order, "Tower" of States, and Symmetry Breaking in Lattice Quantum Systems. *Journal of Statistical Physics* **174**, 735–761 (2019). URL https://doi.org/10.1007/s10955-018-2193-8.

[51] Macrì, T., Smerzi, A. & Pezzè, L. Loschmidt echo for quantum metrology. *Physical Review A* **94**, 010102 (2016). URL https://link.aps.org/doi/10.1103/PhysRevA.94.010102. Publisher: American Physical Society.

[52] Davis, E., Bentsen, G. & Schleier-Smith, M. Approaching the Heisenberg Limit without Single-Particle Detection. *Physical Review Letters* **116**, 053601 (2016). URL https://link.aps.org/doi/10.1103/PhysRevLett.116.053601. Publisher: American Physical Society.

[53] Colombo, S. *et al.* Time-reversal-based quantum metrology with many-body entangled states. *Nature Physics* **18**, 925–930 (2022). URL https://www.nature.com/articles/s41567-022-01653-5.

[54] Yan, B. *et al.* Observation of dipolar spin-exchange interactions with lattice-confined polar molecules. *Nature* **501**, 521–525 (2013). URL http://www.nature.com/articles/nature12483.

[55] de Léséleuc, S., Barredo, D., Lienhard, V., Browaeys, A. & Lahaye, T. Optical Control of the Resonant Dipole-Dipole Interaction between Rydberg Atoms. *Physical Review Letters* **119**, 053202 (2017). URL https://link.aps.org/doi/10.1103/PhysRevLett.119.053202.

[56] Gottscholl, A. *et al.* Initialization and read-out of intrinsic spin defects in a van der Waals crystal at room temperature. *Nature Materials* **19**, 540–545 (2020). URL https://www.nature.com/articles/s41563-020-0619-6.

[57] Chejanovsky, N. *et al.* Single-spin resonance in a van der Waals embedded paramagnetic defect. *Nature Materials* **20**, 1079–1084 (2021). URL https://www.nature.com/articles/s41563-021-00979-4.

[58] Eichhorn, T. R., McLellan, C. A. & Bleszynski Jayich, A. C. Optimizing the formation of depth-confined nitrogen vacancy center spin ensembles in diamond for quantum sensing. *Physical Review Materials* **3**, 113802 (2019). URL https://link.aps.org/doi/10.1103/PhysRevMaterials.3.113802.

[59] Smith, J. M., Meynell, S. A., Bleszynski Jayich, A. C. & Meijer, J. Colour centre generation in diamond for quantum technologies. *Nanophotonics* **8**, 1889–1906 (2019). URL https://www.degruyter.com/document/doi/10.1515/nanoph-2019-0196/html.

[60] Fishman, M., White, S. R. & Stoudenmire, E. M. The ITensor Software Library for Tensor Network Calculations. *SciPost Phys. Codebases* 4 (2022). URL https://scipost.org/10.21468/SciPostPhysCodeb.4.

[61] Gaenko, A. *et al.* Updated core libraries of the ALPS project. *Computer Physics Communications* **213**, 235–251 (2017). URL https://www.sciencedirect.com/science/article/pii/S0010465516303885.

[62] Wallerberger, M. *et al.* Updated core libraries of the ALPS project. URL http://arxiv.org/abs/1811.08331. 1811.08331 [cond-mat, physics:physics].

Methods and Extended Data for "A Universal Theory of Spin Squeezing"

ORDER AND METROLOGY

As discussed in the main text, there is a simple connection between symmetry breaking order and QFI in pure states, since the variance of the order parameter is nothing but a double sum (or integral) of the two-site correlation function. The particular relationship between possible forms of the correlation function and the resulting QFI and sensitivity are summarized in Table I.

Despite the simplicity of the relation between order and QFI, it is somewhat subtle to understand its implications for the metrological utility of states obtained from thermalizing quenches. Most importantly, since we are interested in systems that feature symmetry breaking order, one must recall that thermalization only occurs *within* symmetry sectors (no population is transferred between symmetry sectors). Therefore we think about the dynamics as ocurring in two steps: first, at a short timescale the system undergoes local thermalization so that few-body operators that *do not* connect symmetry sectors reach their equilibrium value; second, over a longer time scale, few-body operators that *do* connect symmetry sectors continue to evolve. The crucial point is that the latter timescale is governed by the typical energy splitting between symmetry sectors, which is exponentially small even in the ground state for systems with discrete symmetry [1]. It is the slow evolution of observables connecting symmetry sectors that yields large QFI, so systems with discrete symmetry breaking will take an exponentially long time to evolve into a state with QFI indicated by Table. I. For continuous symmetries, the gaps between symmetry sectors can be parametrically larger (e.g. $\sim 1/N$ in the $U(1)$ case), so large QFI can be generated at times scaling only polynomially in N. We note that this connection between QFI and order may also be exploited by breaking the symmetry explicitly with a small field, as shown in [2].

Asymptotic Correlation Function		QFI Scaling	Sensitivity Scaling
$\sim e^{-\lvert x-y\rvert/\xi}$		N	$\frac{1}{\sqrt{N}}$
$\sim \frac{1}{\lvert x-y\rvert^p}$	$p > d$	N	$\frac{1}{\sqrt{N}}$
	$d-1 < p < d$	N^{1+p-d}	$\frac{1}{N^{(1+p-d)/2}}$
	$p < d-1$	N^2	$\frac{1}{N}$

TABLE I. Relation between order, QFI and sensitivity in the case of short range, quasi long-range order, and true long-range order. See also [3].

EXTRACTING THE SQUEEZING PHASE DIAGRAM

According to our analysis, the non- squeezing and scalable squeezing phases should be distinguished by a sudden change of the exponent ν from 0 to 2/5, where ν is defined by the large N behavior of the optimum squeezing, $\xi^2_{\rm opt} \sim N^{-\nu}$. However, two types of finite-size effects make it difficult to observe this directly in numerics.

The first challenge is that the system always undergoes some *non-scalable* squeezing at short times [4, 5]. In a regime of modest easy-axis coupling and small system sizes, this early time minimum can actually be quantitatively better than the late time minimum that *scales* with system size. To properly evaluate the squeezing transition, we need to isolate the late-time, scalable squeezing. To this end, we introduce a more nuanced definition of optimal squeezing, $\xi^2_{\rm opt}$, as the smallest value of $\xi^2(t)$ at a local minima in the derivative $\frac{d}{dt}\xi^2(t)$ after the local thermalization time. In the squeezing phase, this definition coincides with the true minimum of $\xi^2(t)$. In the non-squeezing phase, no features of $\xi^2(t)$ scale with system size so $\nu = 0$ regardless of the criteria for selecting a representative squeezing value. Thus, our definition only impacts the observed scaling near the critical point, where it serves to mitigate the influence of the aforementioned early-time squeezing on the analysis.

The second significant finite-size effect is that the linear growth of Var$[Y|Z]$ may not affect the squeezing scaling until one examines very large system sizes (which achieve optimal squeezing at very late times). In more detail, the slope of Var$[Y|Z]$ (in units of its early time value) decreases with effective temperature (in units of the local energy scale). For $J_z \gtrsim 0$, the effective temperature of $|x\rangle$ is so low that one may not see $N^{-2/5}$ scaling until system sizes of millions or tens of millions of spins. Hence, to observe $\nu = 2/5$ in numerics we resort to tuning the temperature *without* changing the local energy scale, by altering the polarization of the initial state [Fig. 3(b,c)]. By contrast, if one increases the temperature by tuning J_z, the local energy scale will simultaneously increase, maintaining the system-size threshold for observing $N^{-2/5}$ scaling at numerically inaccessible system sizes.

We emphasize that, assuming the validity of our semiclassical model, the squeezing *will* scale as $N^{-2/5}$ for sufficiently large systems, since we *do* see linear growth of Var$[Y|Z]$ and its quantum analog [Fig. 3(e)]. It is just not apparent at the system sizes we are able to simulate. Therefore, it is not appropriate to look for $\nu = 2/5$ exactly as a signature of the phase transition. Indeed, in our DTWA numerics to study the transition as a function of J_z in $d = 1, 2$ from $N = [120...10379], L = [11...102]$, starting from the fully polarized $|x\rangle$ state, we essentially always see $\nu = 2/3$ in the squeezing phase.

The above effects make it difficult to propose a definitive scaling function for ν that one could use perform standard finite-size scaling. In lieu of this, we simply identify the critical point as J_z value at which ν becomes significantly greater than 0. More specifically, we fit $\nu(J_z)$ to a piecewise function that consists of a flat "floor" and "ceiling" connected by a linear ramp. In $d = 1$, we estimate of J_c as the center of the ramp, and take the width of the ramp as an estimate of the error. In $d = 2$, we estimate J_c as the *onset* of the ramp, and again use the width of the ramp as an estimate of the error. These slightly different definitions of J_c are justified by the very strong effect of long-range interactions in $d = 1$, which cause ν to trend to 0 very slowly with system size in the disordered phase.

In $d = 3$, ν jumps discontinuously from ≈ 0 at $J_z = -1.0$ to ≈ 0.45 at $J_z = -0.9$, so the squeezing critical point clearly lies in this interval (according to our conjecture, it should be exactly $J_z = -1.0$).

FINITE-TEMPERATURE ORDER PHASE DIAGRAM

Numerical methods

In $d = 1$, for each $\{\alpha, J_z\}$, we perform imaginary time evolution to cool an infinite temperature (purified) matrix product state to the effective temperature of $|x\rangle$ [6]. We then determine $m_{\rm xy}(\alpha, J_z)$ from the resulting density matrix and perform a finite size scaling analysis extract the critical Ising coupling strength, shown in Fig. 1(b). In $d = 2$, the problem is more challenging and we rely on quantum Monte Carlo with worm-type updates [7]. Since it is not possible to cool directly to the effective temperature of $|x\rangle$, we undertake a three parameter search over $\{\alpha, J_z, \beta\}$ (where β is inverse temperature) to determine when the energy density at the critical temperature equals that of $|x\rangle$, yielding the the critical points in Fig. 1(c). See the supplementary material [4] for more details on these numerics in both $d = 1, 2$.

Analytic methods

In addition to these numerical approaches, we develop an analytic approximation for the finite-temperature symmetry breaking transition. The key issue we wish to resolve analytically is whether order, at the effective temperature of the coherent-spin state (CSS) $|x\rangle$, requires $\alpha < 2$ for $J_z < 1$ (as opposed to persisting at $\alpha = 2$). To this end, we focus on the vicinity of $\alpha \lesssim 2d$, $J_z \lesssim 1$ where the system can be modeled as Bose gas, based on previous work in Refs. [8, 9], which were in turn motivated by the exact solution of the Haldane–Shastry spin chain [10, 11]. The key physical intution is that the ground state manifold of the model with SU(2) symmetry contains $|x\rangle$, and with weak anisotropy, $0 \leq \delta \equiv 1 - J_z << 1$, this state remains at a low effective temperature so the relevant equilibrium states are still well described as Gaussian states with few excitations.

Holstein–Primakoff bosonization: using z-vacuum

We perform a Holstein–Primakoff bosonization of the model, assuming the fully polarized state along z-axis as the vacuum and making a large-S approximation:

$$\begin{aligned} S_i^+ &= (2S - b_i^\dagger b_i)^{1/2}\ b_i\ , \\ S_i^- &= b_i^\dagger (2S - b_i^\dagger b_i)^{1/2}\ , \\ S_i^z &= S - b_i^\dagger b_i\ , \end{aligned} \tag{1}$$

where $\sqrt{2S - b_i^\dagger b_i} = \sqrt{2S}\left(1 - \frac{1}{4S} b_i^\dagger b_i + O(1/S)\right)$. This approach may seem surprising, however we observe that it is necessary to choose a vacuum that respects U(1) symmetry in order to capture the ordering transition. Consequently, the vacuum has finite energy density except at the spin-isotropic point, where it is a member of the degenerate ground state manifold. The applicability of this theory away from this point is nontrivial: however, as we shall see, the primary effect of anisotropy is to introduce an energy offset between symmetry sectors, and it does not affect the single-particle dynamics at leading order.

Fourier transforming via $b_i^\dagger = \frac{1}{\sqrt{N}} \sum_{\boldsymbol{q}} e^{-i\boldsymbol{q}\cdot\boldsymbol{r}_i} b_{\boldsymbol{q}}^\dagger$ and defining $\eta(\boldsymbol{q}) = \sum_{\boldsymbol{r}\neq 0} |\boldsymbol{r}|^{-\alpha} e^{i\boldsymbol{q}\cdot\boldsymbol{r}}$, the power-law XXZ Hamiltonian is represented in momentum space as

$$\begin{aligned} H &= S^2 H^{(0)} + S H^{(2)} + H^{(4)} + O(1/S) \,, \\ H^{(0)} &= \text{constant} \,, \\ H^{(2)} &= \sum_{\boldsymbol{q}} b_{\boldsymbol{q}}^\dagger b_{\boldsymbol{q}} (\omega(\boldsymbol{q}) - \delta\eta(0)) \,, \quad \omega(\boldsymbol{q}) \equiv \eta(0) - \eta(\boldsymbol{q}) \,, \\ H^{(4)} &= \frac{1}{8N} \sum_{\substack{\boldsymbol{q},\boldsymbol{q}',\\ \boldsymbol{q}'',\boldsymbol{q}'''}} b_{\boldsymbol{q}}^\dagger b_{\boldsymbol{q}'}^\dagger b_{\boldsymbol{q}''} b_{\boldsymbol{q}'''} \delta(\boldsymbol{q}+\boldsymbol{q}'-\boldsymbol{q}''-\boldsymbol{q}''') \left(\eta(\boldsymbol{q}) + \eta(\boldsymbol{q}') + \eta(\boldsymbol{q}'') + \eta(\boldsymbol{q}''') - 4J_z\eta(\boldsymbol{q}-\boldsymbol{q}'')\right) \,. \end{aligned} \tag{2}$$

As $\boldsymbol{q}$ is a momentum eigenvalue, $\eta(\boldsymbol{q}) = \eta(-\boldsymbol{q}) = \eta(\boldsymbol{q})^*$; so $\eta(\boldsymbol{q})$ is real. We proceed following a standard treatment by minimizing the free energy in the variational manifold of Gaussian states of the form $|\{n_{\boldsymbol{q}}\}\rangle = \prod_{\boldsymbol{q}} (n_{\boldsymbol{q}}!)^{-1/2} (b_{\boldsymbol{q}}^\dagger)^{n_{\boldsymbol{q}}} |\Psi_{\text{vac}}\rangle$, keeping only terms up to $O(1/S)$. The minimization depends only on the effective single particle dispersion $\varepsilon(\boldsymbol{q}) = \frac{\partial\langle H\rangle}{\partial n_{\boldsymbol{q}}}\big|_{n_{\boldsymbol{q}'\neq\boldsymbol{q}}}$, and quite generally obtains the Bose-Einstein distribution [12]. In the disordered phase this results in the self-consistency condition

$$M = \sum_{\boldsymbol{q}} n(\boldsymbol{q}) = \sum_{\boldsymbol{q}} \frac{1}{e^{(\varepsilon(\boldsymbol{q})-\mu)/T} - 1}. \tag{3}$$

We emphasize that Eq. (3) only counts particles in *excited* modes due to the vanishing density of states at $q = 0$. Therefore, while the variational states have fixed particle number M we are able to treat the problem in the *grand canonical* ensemble by allowing the Bose-Einstein condensate to act as a source of particles, whose average is set by μ. Above T_c one can self-consistently determine $\mu < 0$, and we identify T_c as the temperature satisfying Eq. (3) with $\mu = 0$, where exactly M particles are extracted from the condensate into excited modes.

To determine $\varepsilon(\boldsymbol{q})$ explicitly, we apply Wick's theorem and Eq. (3) to find

$$\begin{aligned} \langle H\rangle = \eta(0)\left(-\frac{1}{2}NS^2J_z - \delta\left(SM - \frac{M(M-1)}{2N}\right)\right) + \sum_{\boldsymbol{q}} n(\boldsymbol{q})\left(S - \frac{M-1}{2N}\right)\omega(\boldsymbol{q}) \\ - \frac{1}{2N}\sum_{\boldsymbol{q}} n(\boldsymbol{q}) \sum_{\boldsymbol{q}'\neq\boldsymbol{q}} n(\boldsymbol{q}')(J_z\eta(\boldsymbol{q}-\boldsymbol{q}') - \eta(\boldsymbol{q}')) \,. \end{aligned} \tag{4}$$

From Eq. (4), we can gain further insight into the validity of our approximation away from the Heisenberg point. Specifically, while the anisotropy δ contributes an M-dependent offset leading to a unique ground state sector with $M = SN$, it does not directly modify the quadratic terms. While $|x\rangle$ superposes particle number sectors, the fluctuations are small and we work in the sector $M = \langle M\rangle = SN$. This renders the leading order effect of the anisotropy irrelevant. Moreover, for small anisotropy, which perturbs $|x\rangle$ away from the ground-state manifold, interactions are suppressed, as for low temperature only very low momentum modes have significant occupation. The quartic term is then suppressed by the width of the momentum distribution $n(\boldsymbol{q})$.

Condensation and effective initial temperatures

Based on the above, as an approximation, we discard the interaction term, making H diagonal in $\boldsymbol{q}$. Now there is no remaining $\boldsymbol{q}$-dependent term involving anisotropy, so this result is the same as that of Refs. [8, 9] for the SU(2) model.

To leading order, the estimate of the critical temperature is

$$T_c = \begin{cases} -\dfrac{\pi S}{2\Gamma(\alpha)\cos\left(\frac{\pi\alpha}{2}\right)} \left(\dfrac{\pi S(\alpha-1)}{\Gamma(\frac{1}{\alpha-1})\zeta(\frac{1}{\alpha-1})}\right)^{\alpha-1} & , \quad d = 1 \,, \\ -\dfrac{2^{1-\alpha}\pi^2 S}{\Gamma(\frac{\alpha}{2})^2\sin\left(\frac{\pi\alpha}{2}\right)} \left(\dfrac{2\pi S(\alpha-2)}{\Gamma(\frac{2}{\alpha-2})\zeta(\frac{2}{\alpha-2})}\right)^{\frac{\alpha-2}{2}} & , \quad d = 2 \,. \end{cases} \tag{5}$$

In $d = 1$ the leading behavior as $\alpha \to 2$ from below is $T_c \sim \frac{\pi^2}{2} S^2(2-\alpha)$. In $d = 2$ the critical temperature jumps discontinuously at $\alpha = 4$, from $\lim_{\alpha\to 4} T_c = \frac{\pi^2}{8}$ to 0, as required by rigorous bounds [13].

Using the same picture of the low-energy thermodynamics allows to compute the effective temperature T_0 of the CSS initial state. Its energy is exactly $E_{\rm CSS} = -\frac{N}{8}\eta(0)$, which turns out to be (as $N \to \infty$) the lowest variational energy for $M = SN = \frac{N}{2}$. Given the ground state energy density, we can compute the excitation energy per site of the CSS and relate this to its temperature in the Bose gas. To leading order

$$T_0 = \begin{cases} \left(-\dfrac{\pi S}{2\Gamma(\alpha)\cos\left(\frac{\pi\alpha}{2}\right)}\right)^{\frac{1}{\alpha}} \left(\dfrac{\pi(\alpha-1)\mathcal{E}(\alpha,J_z)}{\Gamma(\frac{\alpha}{\alpha-1})\zeta(\frac{\alpha}{\alpha-1})}\right)^{\frac{\alpha-1}{\alpha}}, & d=1\,, \\ \left(-\dfrac{2^{1-\alpha}\pi^2 S}{\Gamma(\frac{\alpha}{2})^2\sin\left(\frac{\pi\alpha}{2}\right)}\right)^{\frac{2}{\alpha}} \left(\dfrac{2\pi(\alpha-2)\mathcal{E}(\alpha,J_z)}{\Gamma(\frac{\alpha}{\alpha-2})\zeta(\frac{\alpha}{\alpha-2})}\right)^{\frac{\alpha-2}{\alpha}}, & d=2\,, \end{cases} \tag{6}$$

where $\mathcal{E}(\alpha, J_z)$ is the energy density of the CSS in the thermodynamic limit.

To determine $\mathcal{E}(\alpha, J_z)$, we extrapolate results from DMRG on periodic systems of length $N = 64, 96, 128$ using ITensor [14]. This provides an unbiased estimate accounting for all quantum fluctuations, at the cost of only being able to compute T_0 for specific points in the parameter space. To estimate the critical $J_c(\alpha)$ such that $T_0 = T_c$ more precisely, we we use a simple polynomial fit of $\mathcal{E}(\alpha, J_z)$. The resulting phase boundary is shown in gold in Fig. 1(b) of the main text, and shows good agreement with the boundary obtained from MPS numerics, especially as $J_z \to 1$ where this approximation should be most accurate.

DERIVATION OF THE SQUEEZING PARAMETER VIA SEMI-CLASSICAL APPROACH

As discussed in the main text, spin-squeezing dynamics are well described by a semi-classical picture that approximates the quasiprobability distribution as a true probability distribution evolving on the global Bloch sphere. Here, we present an analytical calculation of the optimal squeezing based on this picture. In particular, we derive Eq. (2) of the main text.

The expression of the spin squeezing parameter ξ^2 consists of the mean spin length $\langle X\rangle$ and the minimum variance $\min_{\hat{n}\perp\hat{x}} \mathrm{Var}[\hat{n}\cdot\mathbf{S}]$ in the y-z plane. The latter is of course the smallest eigenvalue of Y, Z covariance matrix,

$$\begin{pmatrix} \langle Z^2\rangle & \langle ZY\rangle \\ \langle YZ\rangle & \langle Y^2\rangle \end{pmatrix}. \tag{7}$$

Therefore, to calculate the squeezing we only need to evaluate the observables $\langle X\rangle$, $\langle Z^2\rangle$, $\langle Y^2\rangle$ and $\langle ZY\rangle = \langle YZ\rangle$.

Since Z is a conserved quantity, we can consider the evolution of each Z-slice of the probability distribution separately. The population within each slice is conserved and determined by the initial binomial distribution of Z, which can be well approximated by a Gaussian distribution in the thermodynamic limit. That is,

$$P(Z) = \sqrt{\frac{2}{\pi N}}\mathrm{e}^{-\frac{2Z^2}{N}}. \tag{8}$$

The dynamics in each Z-slice are then described by a rotation with a angular velocity of $\frac{2Z\chi}{N}$ given as the follows:

$$\begin{aligned} X|Z &= Nm_{\rm xy}\cos\left(\frac{2Z\chi t}{N}\right), \\ Y|Z &= Nm_{\rm xy}\sin\left(\frac{2Z\chi t}{N}\right). \end{aligned} \tag{9}$$

Therefore, all the terms in ξ^2 can be evaluated as

$$\begin{aligned} \langle X\rangle &= \int Nm_{\rm xy}\cos\left(\frac{2Z\chi t}{N}\right)P(Z)dZ = Nm_{\rm xy}\mathrm{e}^{-\frac{(\chi t)^2}{2N}} \\ \langle Z^2\rangle &= \int Z^2P(Z)dZ = \frac{N}{4} \\ \langle ZY\rangle = \langle YZ\rangle &= \int ZNm_{\rm xy}\sin\left(\frac{2Z\chi t}{N}\right)P(Z)dZ = \frac{1}{2}Nm_{\rm xy}\chi t\,\mathrm{e}^{-\frac{(\chi t)^2}{2N}}, \\ \langle Y^2\rangle &= \mathrm{Var}[Y|Z] + \int N^2m_{\rm xy}^2\sin^2\left(\frac{2Z\chi t}{N}\right)P(Z)dZ \\ &= \mathrm{Var}[Y|Z] + \frac{1}{2}N^2m_{\rm xy}^2[1-\mathrm{e}^{-\frac{2(\chi t)^2}{N}}]. \end{aligned} \tag{10}$$

Plugging the above last three lines into Eq. 7, we obtain the minimum variance in the y-z plane as

$$\begin{aligned}\min_{\hat{n}\perp\hat{x}} \mathrm{Var}[\hat{n}\cdot\mathbf{S}] = \frac{1}{2}\left\{\mathrm{Var}[Y|Z] + \frac{N}{4} + \frac{1}{2}N^2 m_{\mathrm{xy}}^2[1-\mathrm{e}^{-\frac{2(\chi t)^2}{N}}]\right\} \\ - \frac{1}{2}\left[\left\{\mathrm{Var}[Y|Z] - \frac{N}{4} + \frac{1}{2}N^2 m_{\mathrm{xy}}^2[1-\mathrm{e}^{-\frac{2(\chi t)^2}{N}}]\right\}^2 + N^2 m_{\mathrm{xy}}^2 \chi^2 t^2 \mathrm{e}^{-\frac{(\chi t)^2}{N}}\right]^{1/2}.\end{aligned} \tag{11}$$

Scalable squeezing occurs at later and later times as N increases, but occurs *before* the quantum Fisher information reaches maximum at $\sim\sqrt{N}$ [15]. Hence we consider the following limit

$$\chi t \to \infty, \qquad \frac{\chi t}{\sqrt{N}} \to 0, \tag{12}$$

and expand the minimum variance in series

$$\min_{\hat{n}\perp\hat{x}} \mathrm{Var}[\hat{n}\cdot\mathbf{S}] = \frac{N}{4}\left\{\frac{\mathrm{Var}[Y|Z]/N}{m_{\mathrm{xy}}^2(\chi t)^2} + \frac{(\chi t)^4}{6N^2} + \mathcal{O}\left[\frac{1}{(\chi t)^2}\right] + \mathcal{O}\left[(\frac{\chi t}{\sqrt{N}})^4\right]\right\}. \tag{13}$$

We note the mean spin length is simply constant in this limit:

$$\langle X\rangle^2 = N^2 m_{\mathrm{xy}}^2\left\{1 + \mathcal{O}\left[(\frac{\chi t}{\sqrt{N}})^2\right]\right\} \tag{14}$$

Combining the above, we obtain Eq. (2) in the main text.

Let us finally remark that the time dependence of the conditional variance $\mathrm{Var}[Y|Z]$ fully determines the scaling behavior of ξ_{opt} and t_{opt} as a function of N. In particular, if $\mathrm{Var}[Y|Z] \propto N(\chi t)^\gamma$ (with $0 \le \gamma < 2$), by minimizing Eq. (2) we expect

$$\xi_{\mathrm{opt}} \propto N^{-2+\frac{8}{6-\gamma}}, \qquad t_{\mathrm{opt}} \propto N^{\frac{2}{6-\gamma}}. \tag{15}$$

HYDRODYNAMIC MODEL FOR THE LINEAR GROWTH OF CONDITIONAL VARIANCE

The linear growth of $\mathrm{Var}[Y|Z]$ in generic squeezing dynamics is the essential difference from the (integrable) one-axis twising case. Here, we provide an analytical calculation, based on a hydrodynamic description of spontaneous symmetry breaking, that predicts this linear growth. Our main assumption is that after a relatively short time (of order $1/J$), the system achieves local thermal equilibrium and the subsequent dynamics of coarse-grained variables can be described by hydrodynamic equations.

The hydrodynamic description focuses on two coarse-grained variables that evolve only slowly in time at long wavelengths, the z-component of the magnetization density, denoted $m(\mathbf{r})$ (the $U(1)$ charge), and an angle $\phi(\mathbf{r})$ describing the orientation of the magnetization in the x-y plane. The magnitude of the in-plane component, m_{xy}, is assumed to have relaxed rapidly to a value determined by the temperature T, which we take to be uniform in space. The phase ϕ will vary slowly at long wavelengths because the restoring force vanishes for long wavelength fluctuations, and m varies slowly because it is a conserved quantity. A hydrodynamic description should apply for sufficiently long wavelengths at any non-zero temperature, regardless of whether the underlying microscopic system obeys classical or quantum dynamics.

Integrating the partition function over short range fluctuations in m and ϕ, and over all other variables in the problem, we may define a free energy functional, which we assume to take the form

$$F[m,\phi] = \int d^d r\, \left(\chi m(\mathbf{r})^2 + u_4 m(\mathbf{r})^4 + ...\right) + \int d^d r_1 d^d r_2 \tilde{J}(\mathbf{r}_1 - \mathbf{r}_2)\left\{\cos[\phi(\mathbf{r}_1) - \phi(\mathbf{r}_2)]\right\}, \tag{16}$$

where $\tilde{J}(\mathbf{r}) \sim (J_\perp/2) m_{\mathrm{xy}}^2 r^{-\alpha}$ for large separations r. The hydrodynamic equations of motion take the form

$$\begin{aligned}\frac{\partial\phi}{\partial t} &= g\frac{\delta F}{\delta m} - \Gamma\frac{\delta F}{\delta\phi} + \eta_\phi(t,\mathbf{r}), \\ \frac{\partial m}{\partial t} &= -g\frac{\delta F}{\delta\phi} + \nabla^2\left[\Lambda\frac{\partial F}{\partial m} + \eta_m(t,\mathbf{r})\right], \\ \langle\eta_\phi(t,\mathbf{r})\rangle &= \langle\eta_\phi(t,\mathbf{r})\rangle = 0, \\ \langle\eta_\phi(t,\mathbf{r})\eta_\phi(t',\mathbf{r}')\rangle &= 2\Gamma T\delta(t-t')\delta(\mathbf{r}-\mathbf{r}'), \\ \langle\eta_m(t,\mathbf{r})\eta_m(t',\mathbf{r}')\rangle &= 2\Lambda T\delta(t-t')\delta(\mathbf{r}-\mathbf{r}'),\end{aligned} \tag{17}$$

where η_ϕ and η_m originate from the thermal fluctuations.In this framework, Var$[Y|Z]$ corresponds to $m_{\rm xy}^2 N^2 {\rm Var}[\Phi|Z]$, where

$$\Phi = \frac{\int d^d\mathbf{r}\phi(\mathbf{r})}{V} \tag{18}$$

is the phase averaged over the entire system, given fixed total magnetization along z-axis,

$$\int m(\mathbf{r})\, d^d r = Z. \tag{19}$$

The coefficient g in the hydrodynamic equations is determined by the commutator of m and ϕ. In the present problem, $g = 1$. Our hydrodynamic equations are a generalization to the case of long-range spin interactions of the hydrodynamic equations that are commonly used for an XY magnet with short-range interactions in two or more dimensions. [16, 17]. It is expected that these equations should be valid at any temperature in the broken symmetry phase at sufficiently long wave lengths. The hydrodynamic equations are also believed to be valid in the low-temperature phase of the two-dimensional system with short range forces, where there is no true broken symmetry but only quasi-long-range order of the x-y magnetization. We do not have a rigorous derivation of these equations starting from the microscopic Hamiltonian, but one can at least perform some consistency checks. For example, one can confirm that non-linear coupling to thermally excited long-wavelength spin fluctuations does not lead to a divergence of the coefficient Γ. We note that the equations of motion conserve the value of M, and they are consistent with a time-independent thermal distribution of the form $P[m,\phi] = \mathcal{Z}^{-1} e^{-F[m,\phi]/T}$.

For small fluctuations about the equilibrium state, where $m = 0$ and ϕ is independent of space, one can solve the dynamics of Eq. (17) by performing a Fourier transform. This leads to the following equations of motion in momentum space

$$\frac{d\phi_{\mathbf{k}}}{dt} = 2g\chi m_{\mathbf{k}} - \Gamma K_{\mathbf{k}}\phi_{\mathbf{k}} + \eta_{\phi,\mathbf{k}}(t) \tag{20}$$

$$\frac{dm_{\mathbf{k}}}{dt} = -gK_{\mathbf{k}}\phi_{\mathbf{k}} - k^2[2\Lambda\chi m_{\mathbf{k}} + \eta_{m,\mathbf{k}}(t)], \tag{21}$$

where $K_{\mathbf{k}}$ is related to $J_{\mathbf{k}}$, the Fourier transform of $\hat{J}$, by

$$K_{\mathbf{k}} = 2(J_0 - J_{\mathbf{k}}). \tag{22}$$

The noise terms satisfy

$$\left\langle \tilde{\eta}_{\phi,\mathbf{k}}(t)\tilde{\eta}^*_{\phi,\mathbf{k}}(t')\right\rangle = \frac{2\Gamma T}{N}\delta(t-t'), \quad \left\langle \tilde{\eta}_{m,\mathbf{k}}(t)\tilde{\eta}^*_{m,\mathbf{k}}(t')\right\rangle = \frac{2\Lambda T}{N}\delta(t-t'). \tag{23}$$

For small wave vectors, one finds $K_{\mathbf{k}} \sim \tilde{K}k^{\alpha-d}$, where the coefficient $\tilde{K}$ is proportional to $J_\perp m_{\rm xy}^2$. Then, for $k \neq 0$, the equations of motion lead to propagating spin waves, with frequency $\omega_{\mathbf{k}} \sim (2g^2\chi K_{\mathbf{k}})^{1/2}$ and a damping rate proportional to $\Gamma K_{\mathbf{k}} + 2\Lambda\chi k^2$.

Crucially, the $k = 0$ mode is different from the other modes. The first term in Eq. (20) just gives a constant precession rate, $2Z\chi/N$ due to fixed total magnetization, and the second term also vanishes for $\alpha > d$. The equation of motion for Φ then reads

$$\frac{d\Phi}{dt} = \tilde{\eta}_\phi(t), \tag{24}$$

which is the stochastic equation for a random walk Thus

$${\rm Var}[\Phi(t)|Z] = {\rm Var}[\Phi(0)] + \frac{2\Gamma T}{N}t \tag{25}$$

This proves the linear growth of Var$[Y|Z] = N^2 m_{\rm xy}^2 {\rm Var}[\Phi(t)|Z]$.

Two remarks are in order. First, the linear growth rate vanishes when temperature $T \to 0$, suggesting that such effect is very weak for the quench dynamics from a low-temperature initial state. This explains why our proposed scaling behavior of squeezing is hard to observe at low temperature. We note that the linear growth rate will probably vanish *faster* then T at low temperature, since the noise strength Γ can also depend on temperature and vanish itself when $T \to 0$. Second, the behavior of the non-zero momentum modes ($k \neq 0$) is qualitatively different from the zero-momentum mode: due to the non-zero restoring force, Var$[\phi_k(t)]$ cannot increase to infinity and will instead saturate to a temperature-dependent equilibrium value. This effect manifests as the evolution towards local equilibration in the quench dynamics.

We remark that the analysis described above is restricted to the case where the z-component of the total magnetization is confined to a small interval about $Z = 0$. At finite value of Z/N, the hydrodynamic description must take into account fluctuations in energy density, which gives rise to an additional slow mode due to energy conservation. Energy fluctuations couple linearly to the spin modes for $Z/N \neq 0$, and this coupling can have significant effects. Because the initial state is a superposition of states with different energies, and these energies persist to infinite times, we expect that in the large N limit, the quantity $\mathrm{Var}[\Phi(t)]$ should grow as t^2/N for large t. This reflects the fact that systems with slightly different total energies will have slightly different values of the parameter χ. For a state where Z/N is of order $N^{-1/2}$, however, the quantity $\mathrm{Var}[\Phi(t)]$ should grow as t^2/N^2 for large t, which is too small to affect the squeezing behavior.

EXTRACTION OF THE EFFECTIVE ONE-AXIS-TWISTING STRENGTH

To compute the quantum analog of the conditional variance $\mathrm{Var_q}[Y|Z]$ from the Loschmidt echo (Eq. 3 of the main text), we need to determine the effective OAT strength χ. Semiclassically, χ is defined so that different m-sectors are rotated back to their original positions. Quantum mechanically, this corresponds to cancelling the relative phase accumulation between two adjacent m-sectors, i.e. we require:

$$\langle m+1|e^{it(H_{\mathrm{xxz}}-\chi\frac{\hat{Z}^2}{N})}\ \hat{Y}\ e^{-it(H_{\mathrm{xxz}}-\chi\frac{\hat{Z}^2}{N})}|m\rangle = 0, \tag{26}$$

where $|m\rangle$ is the projection of $|x\rangle$ into the m-sector. This immediately leads to the expectation:

$$\begin{aligned}\langle m+1|e^{itH_{\mathrm{xxz}}}\ \hat{X}\ e^{-itH_{\mathrm{xxz}}}|m\rangle &\sim \cos(\Delta E\cdot t),\\ \langle m+1|e^{itH_{\mathrm{xxz}}}\ \hat{Y}\ e^{-itH_{\mathrm{xxz}}}|m\rangle &\sim \sin(\Delta E\cdot t),\end{aligned} \tag{27}$$

where ΔE is the relative energy difference between two adjacent m-sectors.To determine ΔE, we compute the left side of Eq. 27 by time evolving $|m\rangle$ and $|m+1\rangle$ with the Krylov subspace method and then fit the data to sinusoid oscillations. We note these oscillations are damped in principle (reflecting the linear growth of $\mathrm{Var_q}[Y|Z]$), but this is neglible in our fits. We then extract χ by fitting $\Delta E = (2m+1)\chi$.

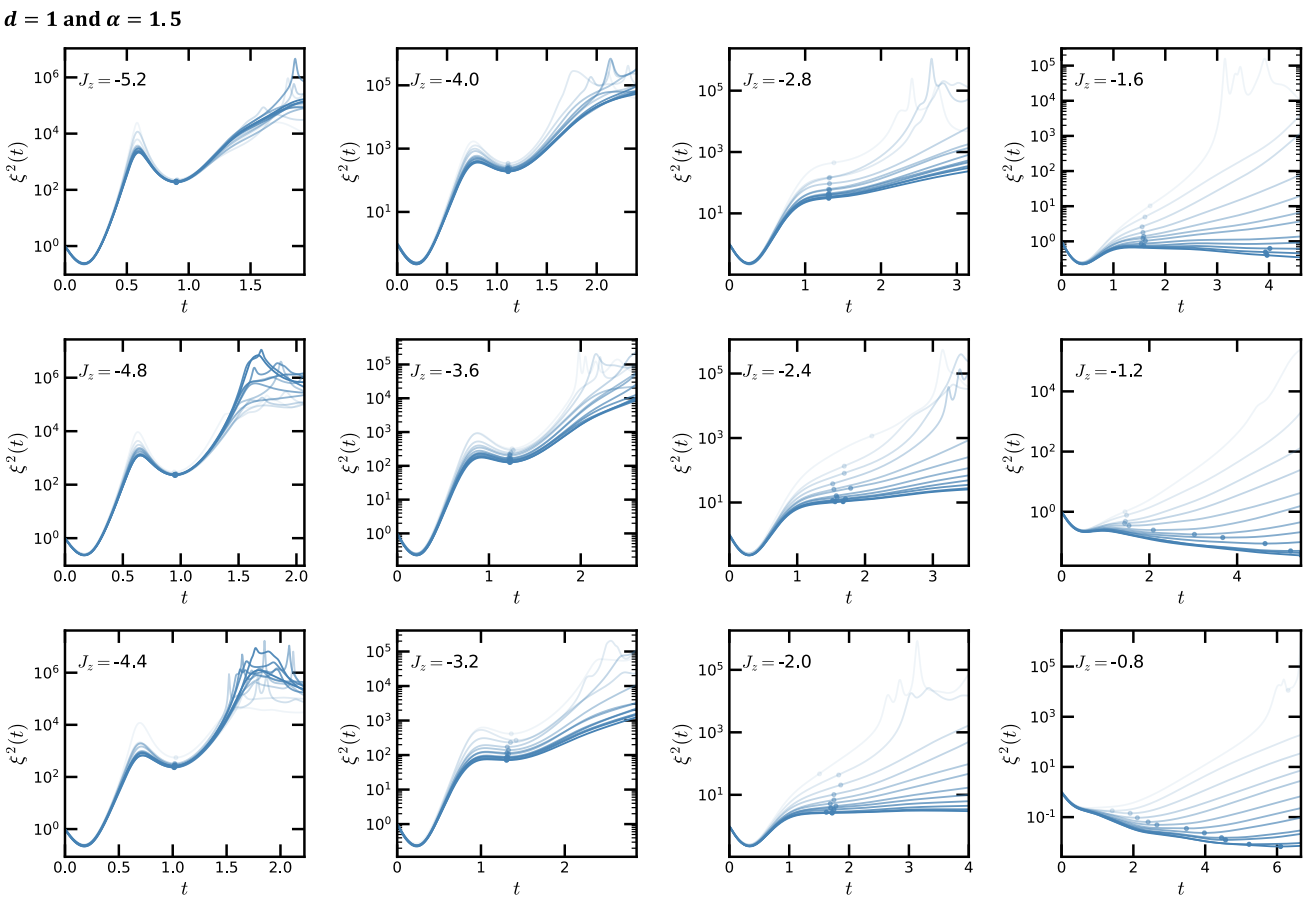

FIG. 1. Squeezing as a function of time from DTWA simulations for $d = 1$ $N = [120...10379]$. Opacity increases with system size. Circular markers indicate the characteristic squeezing $\xi^2_{\rm opt}$ determined via the technique described in the Methods.

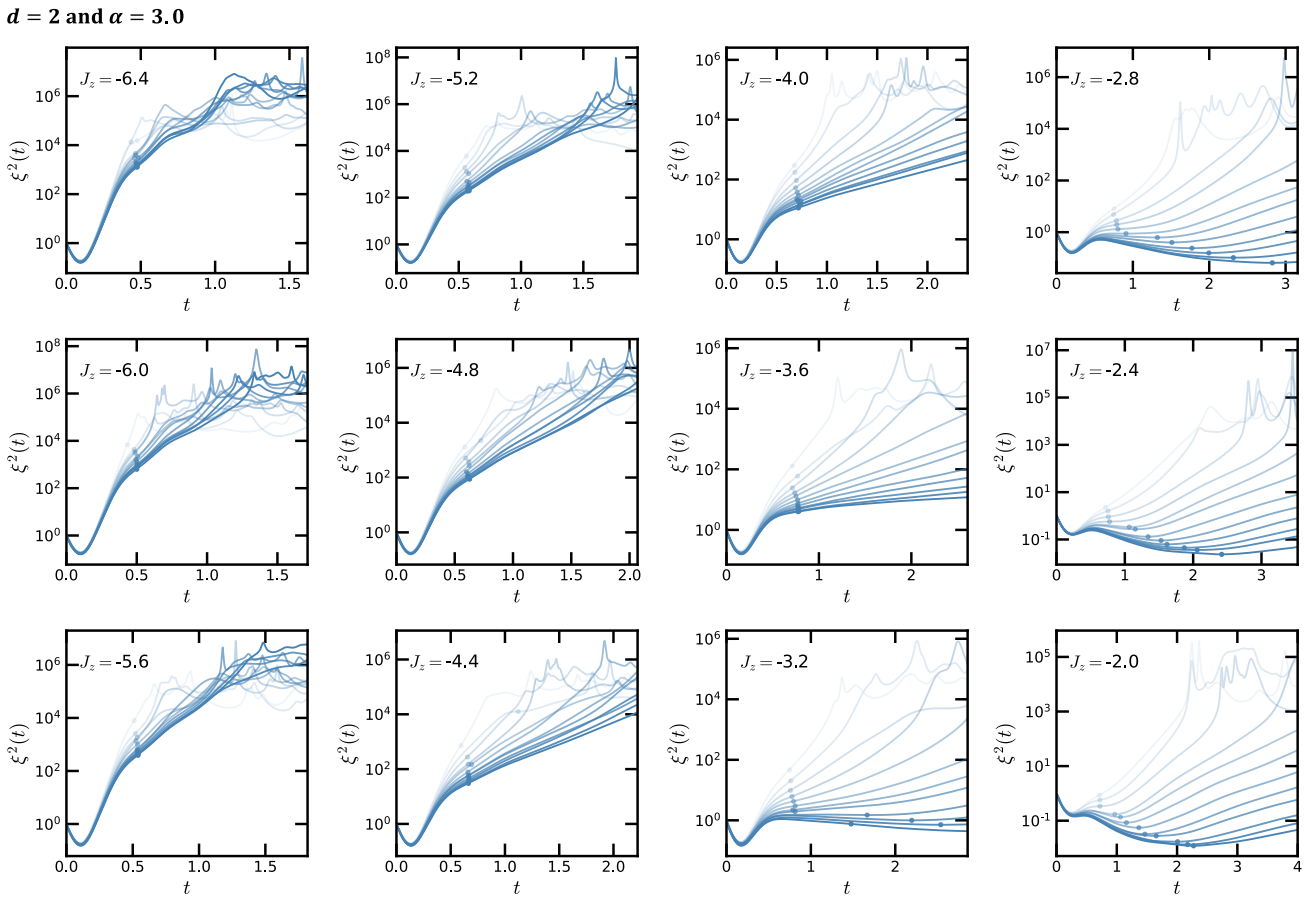

FIG. 2. Squeezing as a function of time from DTWA simulations for $d = 2$ $L = [11...102]$. Opacity increases with system size. Circular markers indicate the characteristic squeezing $\xi^2_{\rm opt}$ determined via the technique described in the Methods.

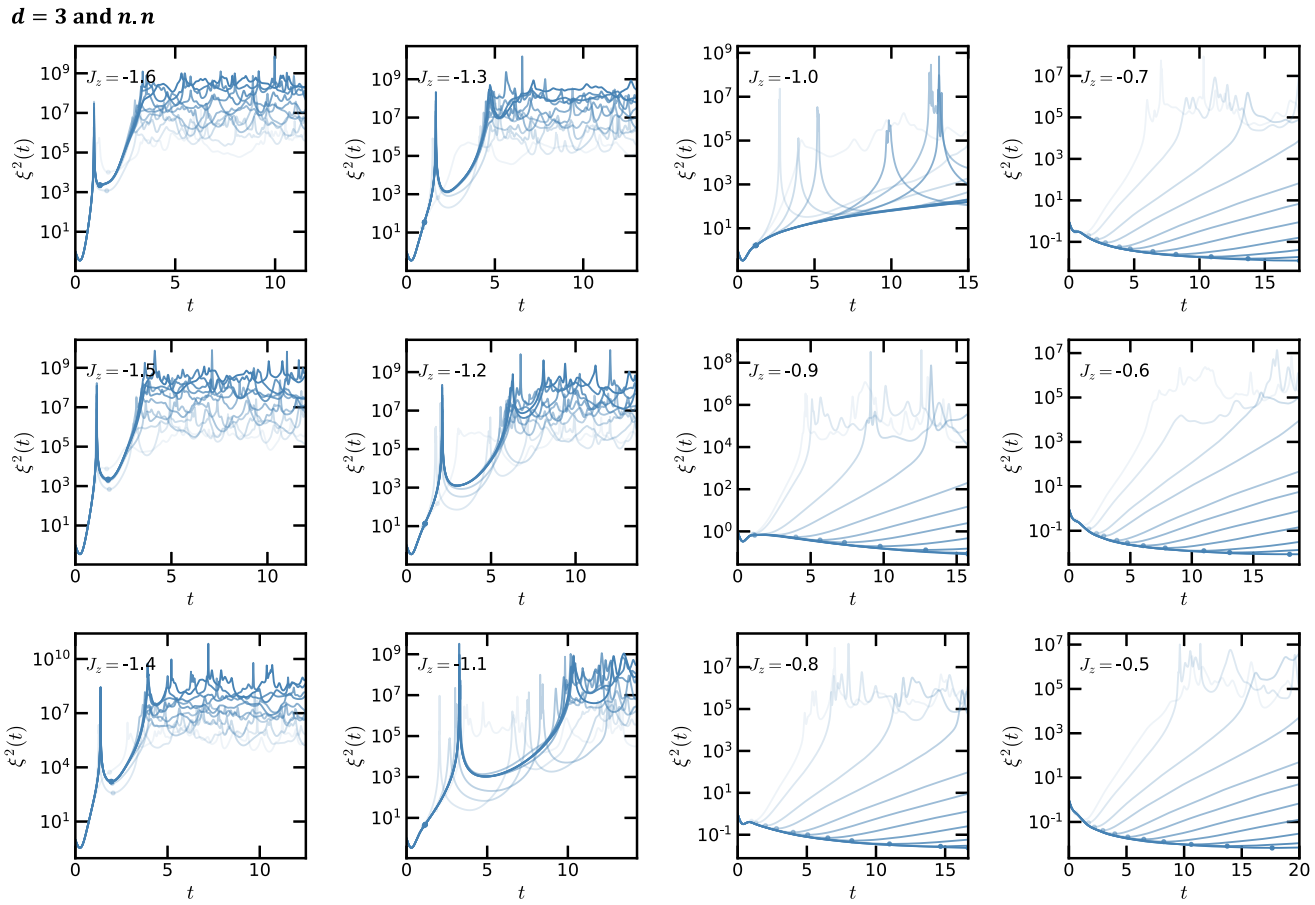

FIG. 3. Squeezing as a function of time from DTWA simulations for $d = 3$ with nearest-neighbor interactions for $L = [5...50]$. Opacity increases with system size. Circular markers indicate the characteristic squeezing $\xi^2_{\rm opt}$ determined via the technique described in the Methods.

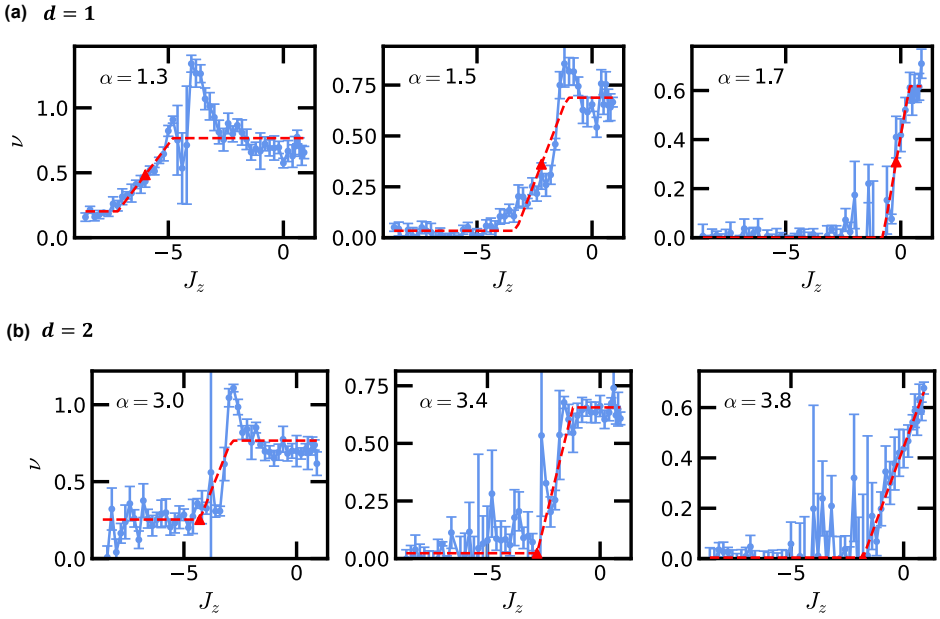

FIG. 4. (a) Squeezing scaling exponent ν as a function of J_z for varying α in $d = 1$. Red dashed curves show piece-wise linear fit used to determine J_c^{sqz} (marked by red triangle), as described in the Methods. (b) Analogous results for $d = 2$. Here, J_c^{sqz} is estimated as the onset of the linear ramp rather than the midpoint. For information on determinign the J_c for finite temperature to which these results are compared [Fig. 1(b,c)], see the supplemental material.

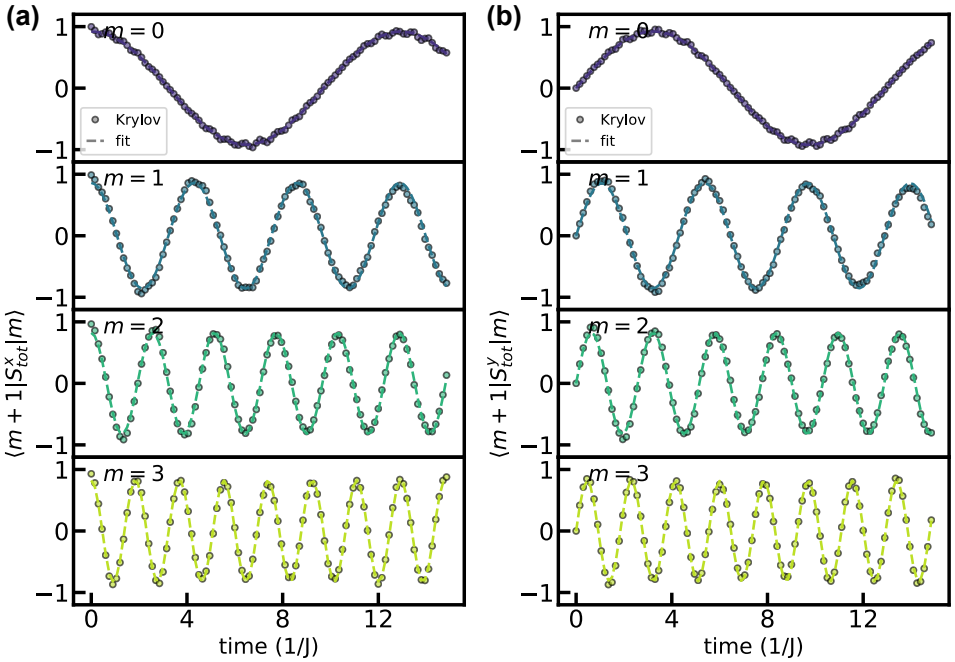

FIG. 5. (a,b) Time-dependent matrix elements of S^x_{tot}, S^y_{tot} respectively used to determine ΔE as described in the Methods. The ΔE are then used to determine χ from $\Delta E = \chi(2m + 1)$.

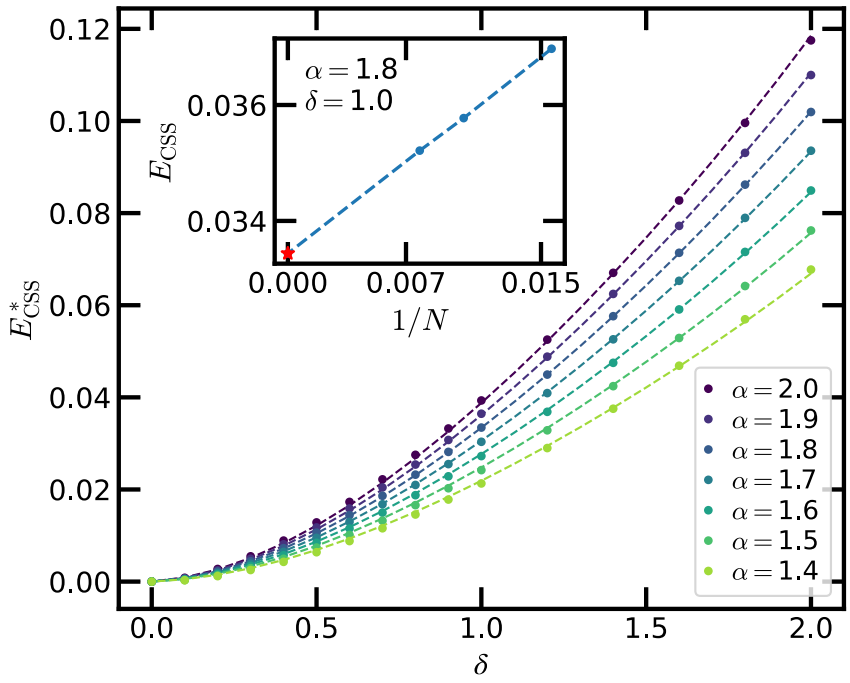

FIG. 6. Interpolations of E^*_{CSS} used to determine phase boundary as described in methods. (inset) Example extrapolation of DMRG results to determine $E^*_{\mathrm{CSS}} \equiv \lim_{N\to\infty} E^N_{\mathrm{CSS}}$.

[1] To see this, note that the generator for a discrete symmetry is an N-body operator, e.g. $\prod_{i=1}^{N} \sigma_i^x$ for a $\mathbb{Z}_2$ Ising model. Then, $O(N)$ few-body terms from H are required to connect symmetry breaking states, resulting in an exponentially gap between the possible symmetry-respecting superpositions.

[2] Comparin, T., Mezzacapo, F., Robert-de Saint-Vincent, M. & Roscilde, T. Scalable Spin Squeezing from Spontaneous Breaking of a Continuous Symmetry. *Physical Review Letters* **129**, 113201 (2022). URL https://link.aps.org/doi/10.1103/PhysRevLett.129.113201.

[3] Frérot, I., Naldesi, P. & Roscilde, T. Entanglement and fluctuations in the XXZ model with power-law interactions. *Physical Review B* **95**, 245111 (2017). URL https://link.aps.org/doi/10.1103/PhysRevB.95.245111. Publisher: American Physical Society.

[4] See Supplemental Material at [URL will be inserted by publisher].

[5] Roscilde, T., Mezzacapo, F. & Comparin, T. Spin squeezing from bilinear spin-spin interactions: Two simple theorems. *Phys. Rev. A* **104**, L040601 (2021). URL https://link.aps.org/doi/10.1103/PhysRevA.104.L040601.

[6] Hauschild, J. & Pollmann, F. Efficient numerical simulations with Tensor Networks: Tensor Network Python (TeNPy). *SciPost Physics Lecture Notes* 005 (2018). URL https://scipost.org/10.21468/SciPostPhysLectNotes.5.

[7] Prokof'ev, N. V., Svistunov, B. V. & Tupitsyn, I. S. Exact, complete, and universal continuous-time worldline Monte Carlo approach to the statistics of discrete quantum systems. *Journal of Experimental and Theoretical Physics* **87**, 310–321 (1998). URL http://dx.doi.org/10.1134/1.558661.

[8] Nakano, H. & Takahashi, M. Quantum heisenberg chain with long-range ferromagnetic interactions at low temperatures. *Journal of the Physical Society of Japan* **63**, 926–933 (1994). URL https://doi.org/10.1143/JPSJ.63.926.

[9] Nakano, H. & Takahashi, M. Quantum heisenberg model with long-range ferromagnetic interactions. *Phys. Rev. B* **50**, 10331–10334 (1994). URL https://link.aps.org/doi/10.1103/PhysRevB.50.10331.

[10] Haldane, F. D. M. Exact jastrow-gutzwiller resonating-valence-bond ground state of the spin-$\frac{1}{2}$ antiferromagnetic heisenberg chain with $1/\mathrm{r}^2$ exchange. *Phys. Rev. Lett.* **60**, 635–638 (1988). URL https://link.aps.org/doi/10.1103/PhysRevLett.60.635.

[11] Haldane, F. D. M. "spinon gas" description of the s=1/2 heisenberg chain with inverse-square exchange: Exact spectrum and thermodynamics. *Phys. Rev. Lett.* **66**, 1529–1532 (1991). URL https://link.aps.org/doi/10.1103/PhysRevLett.66.1529.

[12] Reif, F. *Fundamentals of Statistical and Thermal Physics* (Waveland Press Inc., 2009).

[13] Bruno, P. Absence of spontaneous magnetic order at nonzero temperature in one- and two-dimensional heisenberg and XY systems with long-range interactions. *Phys. Rev. Lett.* **87**, 137203 (2001). URL https://link.aps.org/doi/10.1103/PhysRevLett.87.137203.

[14] Fishman, M., White, S. R. & Stoudenmire, E. M. The ITensor Software Library for Tensor Network Calculations. *SciPost Phys. Codebases* 4 (2022). URL https://scipost.org/10.21468/SciPostPhysCodeb.4.

[15] Comparin, T., Mezzacapo, F. & Roscilde, T. Multipartite entangled states in dipolar quantum simulators. *Phys. Rev. Lett.* **129**, 150503 (2022). URL https://link.aps.org/doi/10.1103/PhysRevLett.129.150503.

[16] HALPERIN, B. I. & HOHENBERG, P. C. Hydrodynamic Theory of Spin Waves. *Physical Review* **188**, 898–918 (1969). URL https://link.aps.org/doi/10.1103/PhysRev.188.898.

[17] Hohenberg, P. C. & Halperin, B. I. Theory of dynamic critical phenomena. *Reviews of Modern Physics* **49**, 435–479 (1977). URL https://link.aps.org/doi/10.1103/RevModPhys.49.435.